The Electrical Activity of Saharan Dust as perceived from Surface Electric Field Observations in Greece

Vasiliki Daskalopoulou[1,2], Sotirios A. Mallios[2], Zbigniew Ulanowski[3,4], George Hloupis[5], Anna Gialitaki[2,6], Konstantinos Tassis[7,8] and Vassilis Amiridis[2]

[1]Department of Physics, Faculty of Astrophysics and Space Physics, University of Crete, Heraklion GR-70013, Greece
[2]Institute for Astronomy, Astrophysics, Space Applications and Remote Sensing, National Observatory of Athens, Athens GR-15236, Greece
[3]Department of Earth and Environmental Sciences, University of Manchester, Manchester M13 9PL, UK
[4]British Antarctic Survey, NERC, Cambridge CB3 0ET, UK
[5]Department of Surveying and GeoInformatics Engineering, University of West Attica, Aegaleo Campus GR-12244, Greece
[6]Laboratory of Atmospheric Physics, Department of Physics, Aristotle University of Thessaloniki, Thessaloniki GR-54124, Greece
[7]Department of Physics, and Institute for Theoretical and Computational Physics, University of Crete, Heraklion GR-70013, Greece
[8]Institute of Astrophysics, Foundation for Research and Technology-Hellas, Heraklion GR-71110, Greece

Correspondence to: Vassilis Amiridis (vamoir@noa.gr)

Abstract. We report on the electric field variations during Saharan dust advection over two atmospheric remote stations in Greece, using synergistic observations of the vertical atmospheric electric field strength (E_z) at ground and the lidar-derived particle backscatter coefficient profiles. Both parameters were monitored for the first time with the simultaneous deployment of a ground-based field mill electrometer and a multiwavelength lidar system. The field mill timeseries are processed to extract the diurnal variations of the Global Electric Circuit and remove fast field perturbations due to peak lightning activity. In order to identify the influence of the elevated dust layers on the ground E_z, we extract a Localized Reference Electric Field from the timeseries that reflects the local fair weather activity. Then, we compare it with the reconstructed daily average behaviour of the electric field and the Saharan dust layers' evolution, as depicted by the lidar system. Reported cases of enhanced vertical electric field for detached pure dust layers suggest the presence of in-layer electric charges. Although higher dust loads are expected to result in electric field enhancement, episodic cases that reduce the electric field are also observed. To quantitatively approach our results, we examine the dependency of E_z against theoretical assumptions for the distribution of separated charges within the electrified dust layer. Electrically neutral dust is approximated by atmospheric conductivity reduction, while charge separation areas within electrically active dust layers are approximated as finite extent cylinders. This physical approximation constitutes a more realistic description of the distribution of charges, as opposed to infinite extent geometries, and allows for analytical solutions of the electric field strength, so that observed electric field variations during the monitored dust outbreaks can be explained.

35 **Keywords:** Dust Electrification; Atmospheric Electric Field Measurements; Reference Electric Field; Charge Separation;

1 Introduction

The Global Electric Circuit (GEC) is an electrical circuit, and specifically a spherical capacitor that is formed between two conducting planes, with one being the Earth's surface, a good conductor of electricity, and the other the Ionosphere, a weakly-ionized plasma at ~80 km altitude (e.g., Rycroft et al., 2008). Atmospheric electric parameters, such as the vertical Electric

40 Field (E_z) and induced air to Earth current (I_c) through the GEC, greatly depend on ambient weather conditions and convective meteorological systems due to the re-distribution of charged or uncharged aerosols and terrestrial radioactive particles in the Earth's atmosphere (e.g. Harrison & Ingram, 2005; Scrase, 1935; Wright, 1933). Under fair weather conditions, which are defined according to international standards as those with cloudiness less than 0.2, wind speed less than 5 m/s and the absence of fog or precipitation (Chalmers, 1967; Harrison & Nicoll, 2018), the atmospheric electrical circulation is dominated by the

45 potential difference between the global capacitor planes (about 250 kV, e.g., Rycroft et al., 2008), which in turn generates the fair weather electric field, and consequently the fair weather electric current in the presence of the conducting atmosphere. An average current density of 2 pA/m^2 and a downward looking (by convention positive, e.g., Rakov & Uman, 2003, pp.8) electric field equal to a typical value of about 130 V/m are expected, respectively (Rycroft et al., 2008). The daily variation of the global thunderstorm activity modulates the electric field strength and the resulting diurnal variation is represented by the

50 Carnegie curve (Harrison, 2013).

Among the aerosols affecting the atmospheric electrical content (Whitby & Liu, 1966), mineral dust represents one of the most significant contributors, along with volcanic ash (Harrison et al., 2010), due to its mineralogical composition that results in different electrical properties of the dust particles (Kamra, 1972) and its abundance in terms of dry mass (Tegen et al., 1997). During dust storms, dust devils and subsequent advection of elevated dust layers the electrical parameters can vary greatly

55 from the values under fair weather conditions (Harrison et al., 2016; Renno & Kok, 2008; Zheng, 2013). It is well documented that over deserts the emission process of dust particles can generate large atmospheric electric fields (Esposito et al., 2016; Renno and Kok, 2008; Zheng, 2013) that affect their flow dynamics (Kok and Renno, 2006). Charged dust occurrences are recorded via ground-based methods also in destinations further away from the source (Harrison et al., 2018; Katz et al., 2018; Silva et al., 2016; Yair et al., 2016; Yaniv et al., 2017), while balloon-borne observations (Kamra, 1972; Nicoll et al., 2011)

60 indicate that space charge is indeed persistent within lofted dust layers during their transport to long distances. The exact mechanisms that would explain and sufficiently describe the long-range electrification of dust are not clear yet and remain under investigation. Major processes that are considered responsible for the electrification of dust particles include ion attachment (Tinsley and Zhou, 2006) and particle-to-surface or particle-to-particle collisions, i.e. triboelectrification (Kamra, 1972; Lacks and Shinbrot, 2019; Waitukaitis et al., 2014). Such processes are claimed to have large impact on desert dust

65 lifecycle and its influence, such as the observed particle vertical orientation with impact on radiative transfer (Bailey et al., 2008; Ulanowski et al., 2007) and the retention of larger dust particles in the atmosphere (van der Does et al., 2018; Ryder et al., 2018).

Ground-based electric field measurements can be indicative of the electrical behaviour of elevated dust layers. These measurements can provide useful information if they are combined with other retrievals on aerosol profiling (e.g. lidar).

70 However, features of E-field timeseries, such as the enhancement of the near-ground electric field during dust outbreaks, are still unexplained in broad literature (Yaniv et al., 2016, 2017). Observations of enhanced or even reversed E-field at the height of the ground-based sensor, e.g. an electrostatic fieldmeter, are attributed by Ette (1971) and Freier (1960) to charge separation within electrically active dust. According to several laboratory studies (Duff and Lacks, 2008; Forward et al., 2009; Inculet et al., 2006; Waitukaitis et al., 2014), charge transfer processes lead to smaller particles being negatively charged while larger

75 particles tend to be positively charged, therefore charge separation within lofted dust layers is also possible due to the expected size selective gravitational settling that could stratify the fine and coarse mode particles (Ulanowski et al., 2007). An observed reduction of the E-field in a mountainous area is attributed to the superposition of two dust layers in different heights with respect to the ground-based sensor (Katz et al., 2018). Moreover, layers that exhibit large particle densities lead to more particles competing for the same amount of ions (ion-particle competition, e.g. Gunn, 1954; Reiter, 1992), hence they act as a

80 passive element within the atmospheric circulation and can reduce the near-ground electric field. A similar reduction of the electric field is also expected when meteorological conditions create random particle movement that cancels out the vertical propagation and, subsequently, the stratification of charges. Nonetheless, systematic profiling measurements are needed so as to fully characterize the electrical properties of the dust particles aloft with respect to the locally occurring meteorological conditions.

85 In this study, we focus on monitoring perturbations of the E-field near the ground caused by the transported dust layers, with special emphasis on slow E-field perturbations (with period larger than 6 hours), and we attempt to classify and comment on the electrical activity of the dust layers. As electrically active we define the layers that exhibit charge separation and behave as electrostatic generators in the GEC, similarly to electrified shower clouds and thunderstorms (e.g. Mallios & Pasko, 2012). Conversely, electrically neutral are assumed to be the layers with no charge separation which, therefore, act as passive elements

90 in the GEC, similarly to the non-electrified shower clouds (e.g. Baumgaertner et al., 2014). Four selected cases of Saharan dust plumes are examined, as captured over Finokalia and Antikythera atmospheric observatories by the ground-based electrometer, as well as by the sophisticated Polly[XT] lidar system. In section 2, we provide an overview of the instrumentation and measurement techniques, and specify the methods used to parameterize the electrical behaviour of the dust layers. In section 3, the E-field diurnal variation (relative to the local reference field) is presented along with the dynamic evolution of

95 the dust episodes as revealed by the profiling information from the lidar. We further discuss whether the configuration of finite cylindrical charge accumulation regions, previously suggested for the representation of charge distributions within thunderclouds (Krehbiel et al., 2008; Riousset et al., 2007), is capable of reproducing our experimental results. Finally, we present our conclusions in section 5.

Atmospheric
Chemistry
and Physics
Discussions

2 Data and methodology

100 We analyse four Saharan dust outbreaks recorded over two observational sites in Greece. The first atmospheric monitoring station is situated in the remote location of Finokalia (35.338° N, 25.670° E) on the north eastern coast of Crete, with the nearest large urban center being the city of Heraklion located 70 km to the west. The station is located at the top of a hill (252 m asl) facing the sea within a sector of 270° to 90° and the climatic characteristics are typical of the eastern Mediterranean basin exhibiting two distinctive seasons, the dry season (April to September) characterized by increased levels of pollution

105 and biomass burning and the wet season (October to April). Significant Saharan dust transport occurs when S/SW winds are prevalent during the intermediate season and may lead to ground concentrations exceeding 1 mg/m^3 (Solomos et al., 2018). Since there is no significant human activity occurring at a distance shorter than 15 km within the above sector, it makes it an appropriate location for monitoring dust layers advected directly from the Sahara. The second site is the PANhellenic GEophysical observatory (PANGEA) in the remote island of Antikythera (35.861° N, 23.310° E, 193 m asl). The island covers

110 an area of just 20.43 km^2, 38 km south-east of the larger island of Kythera and is devoid of human activity as its inhabitants are at most twenty people during early fall to mid-summer. The station location is ideal as the island is placed at a crossroad of air masses (Lelieveld et al., 2002), with NNE winds being prominent between August and February, while in spring and early summer western airflows that favor dust transport are observed. Moreover, the prevailing meteorological conditions on the island are again representative of the eastern Mediterranean with warm and dry days in summer in contrast to winter, when

115 the days are colder and wetter days are typical. The dust outbreaks recorded were on the 25th of July 2017 and March 16th 2018 on Finokalia, October 20th 2018 and June 23rd 2019 on Antikythera, selected due to the presence of elevated dust layers in the lidar profiles.

2.1 Aerosol monitoring and characterization

2.1.1. Lidar measurements

120 For the comprehensive characterization of dust particle optical properties, we exploit the vertical profiling capabilities of the Polly[XT] Raman scattering lidar (Engelmann et al., 2016) of the National Observatory of Athens (NOA), as part of the European Aerosol Research Lidar Network (EARLINET). This multiwavelength system is equipped with three elastic channels at 355, 532 and 1064 nm, two rotational/vibrational Raman channels at 387 and 607 nm, two linear depolarization channels at 355 and 532 nm, and one water vapour channel at 407 nm. Combined use of its near-field and far-field telescopes provides reliable

125 vertical profiles from 0.25 km to 10 km in height. The basic lidar quantities used for the monitoring of dust loads and as much as possible pure ones, are the Total Attenuated Backscatter coefficient (1/msr) at 1064 nm (calibrated and range-corrected signal) for lofted particle concentrations and the calibrated Volume Linear Depolarization Ratio (VLDR) at 532 nm for the characterization of aerosol types. VLDR is defined as the ratio of the cross–polarized to the parallel-polarized backscattered signal (Freudenthaler et al., 2009) and typical pure dust values are between 30% - 40% (Haarig et al., 2017).

2.1.2 Ancillary aerosol and trajectory information

The Aerosol Optical Depth (AOD) was monitored by a CIMEL sunphotometer, part of the Aerosol Robotic Network (AERONET - https://aeronet.gsfc.nasa.gov/), which was co-located with the lidar on both stations. For the cases examined here, the AOD varied from 0.221 to 0.366 at 500 nm. To characterize the air masses in regard to their origin we use the NOAA HYSPLIT back trajectory model, driven by GDAS meteorological data (https://www.ready.noaa.gov/HYSPLIT.php). The arrival heights for dust over the observational sites were selected in HYSPLIT according to the prevailing layering depicted by our lidar measurements (Fig. 1).

2.2 Electric Field measurements and data processing

2.2.1. Ground-based E-Field measurements

The JCI 131 Field mill (FM) electrometer (Chubb, 2014; Chubb, 2015) was installed in Finokalia from April 2017 until May 2018 (382 days) and then re-located to Antikythera, where the examined timeseries span from June 2018 to June 2019 (243 days) for continuous monitoring of the near-ground (on instrument mast height) vertical electric field. Field mills are robust instruments, mostly used for lightning warning applications providing, though, sufficient sensitivity for the detection of weaker electric fields. The instrument was mounted on a 3 m pole, and as far as possible from physical obstacles, buildings and any metallic objects that could create distortions to the electric field. However, on Finokalia the FM was on the edge of a hilly elevation which added a topography factor, not quantified in the specific research due to the lack of typical flat ground measurements in the area. On Antikythera, the mill installation location could be more carefully selected to avoid orography, obstacles and power grid lines. Instrument output range was set to the most sensitive scale (2.0 kV full scale) with a sensitivity of the order of 1 V/m for 1 Hz measurement frequency and the data were acquired from a 24-bit local data-logger. In order to interpret the field mill measurements, it is essential to compare the data with a reference field representative of local fair weather conditions. The methodology followed for this process is described in the paragraph below.

2.2.2. Derivation of the Localized Reference Electric Field

For the classification of the behaviour of the vertical electric field under dust influenced conditions, as that of an enhanced, reduced or reversed E-field, comparison with the local long-term fair weather electric field is required. For this purpose, a Localized Reference Electric Field (LREF) is constructed with respect to the local fair weather conditions, prevalent for each station. The specific reference field represents the electric field behavior under local fair weather conditions, which are determined by exploiting only the timeseries inherent attributes, and is derived through the following processing chain (Fig. 2). Instead of eliminating meteorological disturbances (except for lightning activity) for the retrieval of the fair weather E-field information, the local fair weather days are classified as the less electrically disturbed days, based on the measured quantity itself through the construction of this reference field. Although, the local effects on the E_z at each site can be of random nature (wind gusts, lightning strikes, radon emission and turbulent flows due to orography), the selection of fair weather data can be

based on the reduction of random local noise by first removing values which are clearly dominated by local influences (Harrison & Nicoll, 2018).

The FM data are pre-processed by applying the appropriate scaling factor for the 3 m mounting mast of the electrometer (Chubb, 2015) and then days with no missing values due to either instrument malfunction, power outages or pc communication

165   failures, are selected (Filter no.1). Under local fair weather conditions, the E-field, as measured here, is positive therefore imposing the second filtering step with a non-negativity constraint (Filter no. 2). Consequently, the averaged 1s data to 1-minute data (datalogger configuration) are shifted to the frequency domain through a Fast Fourier Transform (FFT) representation so as to evaluate the relative contributions of the first five principal harmonics to the diurnal cycle of the electric field (Harrison, 2013). We note, that days with missing data are removed, because the uneven temporal distribution of the

170   measurements modifies the time window for the FFT algorithm, and therefore, modifies the timeseries spectrum. These are depicted in the following signal equation for $S(t)$:

$$S(t) = A_0 + A_1 \cos(2\pi f_1 t + \varphi_1) + A_2 \cos(2\pi f_2 t + \varphi_2) + A_3 \cos(2\pi f_3 t + \varphi_3)$$
$$+ A_4 \cos(2\pi f_4 t + \varphi_4) \tag{1}$$

where S is the electric field at time t in hrs, A_i for $i = 0, ..4$ where A_0 represents the mean value (constant, zeroth harmonic) and A_1 to A_4 (first to fourth harmonic) represent the amplitudes of the 24, 12, 8, and 6-hour variations, $f_i = i\frac{t}{24}360°$ is the

175   frequency of each harmonic, where $f_0 = 0$ and φ_i are the respective phases in degrees, with $\varphi_0 = 0$ (Harrison, 2013). Based on the form of the Carnegie curve, and assuming that this trend should be followed by the reference field as well, we find empirically that the ratio between the zeroth harmonic and the first harmonic is around 2. Therefore, the E_z values for which the amplitude A_0 is larger than two times the amplitude A_1 are kept (Filter no. 3). The same filter is applied to the other harmonics as well (A_0 is larger than two times the A_i), making sure that not fast transient contribution is kept.

180   Lastly, since the amplitude of each harmonic is expected to be constant for all days (as the amplitudes in the Carnegie curve do), we impose the Chauvenet criterion on each of the filtered five harmonics amplitude, so as to detect outliers. The criterion is imposed once with the use of the relation below:

$$N \, erfc\left(\frac{d^j}{\sqrt{2}s}\right) < \frac{1}{2} \tag{2}$$

for a deviation of:

$$d^j = \left|A_i{}^j - \bar{A}_i\right|$$

185   where $i = 0, ..4$ refers to the ith harmonic, $j = 0, ..N$ day number and N the total number of days, for

$$\bar{A}_i = \frac{1}{N}\sum_{j=1}^{N} A_i{}^j$$

where A_{ij} is the ith harmonic amplitude per day and summated over j gives $\bar{A}_i$ as the mean amplitude of each harmonic. Lastly, erfc(x) is the complementary error function, defined as:

$$erfc(x) = 1 - erf(x) = 1 - \frac{2}{\sqrt{\pi}} \int_0^x e^{-t^2} dt$$

190   Also s is the unbiased sample variance and is defined as:

$$s^2 = \frac{\sum_{j=1}^N \left(A_i{}^j - \bar{A}_i\right)^2}{N - 1}$$

After the Chauvenet criterion is met, 152 total undisturbed weather days are detected for Finokalia and 109 days for Antikythera. From this reduced dataset, we reconstruct the LREF by keeping the mean values of the first three harmonics and calculate the respective standard errors as $\pm 2SE$ from the reconstructed signal.

195   2.2.3. E-field measurement comparison

In order to compare LREF with the daily variation of the electric field during the dust events, these field mill measurements are also shifted to the frequency domain through an FFT. Again, the first five harmonics are retained and from the specific dataset, a smoothed slow varying field is reconstructed (otherwise referred to as reconstructed mean for the remainder of this paper) from the set of mean amplitudes and phases of the first three harmonics. This filtered field retains the main

200   characteristics of the local reference field., since fast transient events which are less than 6 hrs in duration are removed. Therefore, the LREF and reconstructed mean field signals that are compared have the same spectral information. In order to plot the E-field timeseries with the total attenuated backscatter coefficient, all the data are further averaged to 5 mins.

2.3 Mathematical formalism for the modelling of the ground E-field

Under fair weather atmospheric conditions, complete lack of particles in the atmospheric circulation is expected, except of

205   ions. In the steady state of such an atmosphere, the divergence of the total current is zero $\vec{\nabla}\vec{J}_{tot} = 0$, as a direct consequence of the continuity equation and hence the conduction current remains constant with altitude. From Ohm's law, we can relate the conduction current with the vertical component of the electric field (Fig. 3a), as:

$$J_z = \sigma E_z \tag{3}$$

where σ is the atmospheric conductivity and assume a smooth conductivity profile along the altitude z, as:

$$\sigma = \sigma_0 \, exp\left(\frac{z}{l}\right) \tag{4}$$

for σ_0 and l the constants that represent the near ground atmospheric conductivity and the atmospheric scale height

210   respectively.

We, then, express the conduction current at ground level, J_{z_0}, as a function of the columnar resistance R_c and the potential difference $\Delta V = V_{ion} - V_0$, where V_{ion} is the ionospheric potential at the altitude H, and V_0 is the potential at the Earth's surface which is considered a good conductor due to soil particles that are usually covered by a thin, conducting film of water (Kanagy and Mann, 1994), hence V_0 is set equal to zero. Therefore:

$$J_{z_0} = \frac{V_{ion}}{R_c} \tag{5}$$

215   The columnar resistance can be calculated from the conductivity profile of equation (4) (Rycroft et al., 2008), hence:

$$R_c = \int_0^H \frac{dz}{\sigma} = \frac{l}{\sigma_0}\left(1 - exp\left(-\frac{H}{l}\right)\right) \tag{6}$$

By combining equations (3), (5) and (6), the fair weather electric field at ground level is of the form (Gringel et al. 1986):

$$E_{z_0} = \frac{V_{ion}}{\sigma_0 R_c} = \frac{V_{ion}}{l\left(1 - exp\left(-\frac{H}{l}\right)\right)} \tag{7}$$

which depends solely on the scale height l and the ionospheric potential V_{ion}.

However, the presence of dust particles in the atmosphere affects atmospheric conductivity. Neutral aerosols, such as uncharged dust particles, tend to scavenge smaller ions which in turn favours the production of larger ions in expense to the

220   smaller ones (Fuchs, 1963). Since larger ions are less electrically mobile, this attachment process decreases the atmospheric conductivity. The case of a steady state atmospheric desert dust layer that does not exhibit charge stratification is examined below. The layer acts as a passive element and reduces the fair weather atmospheric conductivity by a varying reduction factor n. Fig. 3b, represents the above layer configuration, where the new conductivity profile within the layer will be:

$$\sigma' = \frac{\sigma_0}{n} exp\left(\frac{z}{l}\right) \tag{8}$$

The electric field at ground due to the dust layer, $E_{z_0,layer}$, is given by:

$$E_{z_0,layer} = \frac{V_{ion}}{\sigma_0 R_c'} \tag{9}$$

225   with the columnar resistance being:

$$R_c' = \int_0^{z_1} \frac{dz}{\sigma} + \int_{z_1}^{z_1} \frac{dz}{\sigma'} + \int_{z_1}^H \frac{dz}{\sigma}, \qquad z \neq z_{1,2} \quad \Rightarrow$$

$$R_c' = \frac{l}{\sigma_0}\left[1 + (n-1)exp\left(-\frac{z_c - d/2}{l}\right)\left(1 - exp\left(-\frac{d}{l}\right)\right) - exp\left(-\frac{H}{l}\right)\right] \tag{10}$$

And (9) gives through (10):

$$E_{z_0,layer} = \frac{V_{ion}}{l\left[1 + (n-1)exp\left(-\frac{z_c - d/2}{l}\right)\left(1 - exp\left(-\frac{d}{l}\right)\right) - exp\left(-\frac{H}{l}\right)\right]} \tag{11}$$

where $z_{1,2}$ are the layer bottom/top heights, z_c is the mean layer central height, d is the mean layer depth and R is the layer horizontal extent (radius) which is assumed to be at least ten times larger than its vertical extent ($R \geq 10d$). Therefore, it is clear that $E_{z_0,layer}$ depends on the scale height parameter l, the reduction parameter n, the layer central height z_c and the layer

230   depth $d = z_2 - z_1$. This dependence is further investigated in Section 3.3.1.

On a next step, we parameterize an electrically active dust layer to calculate its impact on the surface E-field. Specifically, we construct a simplistic model for the atmospheric column (1D), based on the hypothesis that the charge accumulation areas within the dust layer can be approximated by charged cylinders of a total charge density $\pm\rho$ (Fig. 3c). For the cylinder, we assume that its horizontal extent, as represented by the cylinder radius, is 10 times larger than the vertical extent, to simulate

235 horizontally homogeneous charge distributions. The electric field of such an idealized finite extent charged layer is dependent on the distance from the layer, with the field lines having only weak radial dependence directly below the center of the layer. Departures from this behaviour occur near layer edges and distances comparable to the layer extent. The hypothesis of image charges is also applied due to the ground being a good conductor, ensuring that the calculated electric potentials are solutions to the Poisson equation.

240 The formulation for such an electrically active layer consists of a superposition of the electrically neutral dust layer case with the monopole charged cylinder case, constrained for zero ground and zero ionospheric potentials. The derivation of the ground electric field due to the presence of a total charge density of ρ is given below. We calculate the potential at point A (central lower point of the charged cylinder), as specified in Fig. 3c, which is given as the sum of the potential from Q and the potential from its image Q_{img}, where $Q_{img} = -Q$:

$$V_A = V_Q + V_{Q_{img}} \tag{12}$$

245 The solution for the potential at the central axis of a solid charged cylinder with total charge density ρ_1, is given by (e.g. Griffiths Instructor's Solutions Manual):

$$V_Q = \frac{\rho_1}{4\varepsilon_0}\left\{ d_1\sqrt{R_1{}^2 + d_1{}^2} + R_1{}^2 \ln\left[\frac{d_1 + \sqrt{R_1{}^2 + d_1{}^2}}{R_1}\right] - d_1{}^2 \right\}, \qquad for\ R_1 \geq 10d_1 \tag{13}$$

where ε_0 is the permittivity of vacuum, R_1 the charge region horizontal extent presented by the cylinder radius, $d_1 = z_2{}' - z_1{}'$ the cylinder depth (charge region vertical extent) and ρ_1 is the total charge density. Correspondingly, the potential at point A due to the image charge is calculated as:

$$
V_{Q_{img}} = \frac{-\rho_1}{4\varepsilon_0}\left\{ 2z_{c_1}\sqrt{R_1{}^2 + \left(2z_{c_1}\right)^2} - \left(2z_{c_1} - d_1\right)\sqrt{R_1{}^2 + \left(2z_{c_1} - d_1\right)^2} \right.
$$

$$
\left. + R_1{}^2 \ln\left[\frac{2z_{c_1} + \sqrt{R_1{}^2 + \left(2z_{c_1}\right)^2}}{\left(2z_{c_1} - d_1\right) + \sqrt{R_1{}^2 + \left(2z_{c_1} - d_1\right)^2}}\right] - 2d_1\left(2z_{c_1} - \frac{d_1}{2}\right) \right\} \tag{14}
$$

250 The new columnar resistance up to the height of point A will be:

$$R_{c_1} = \int_0^{z_1}\frac{dz}{\sigma} + \int_{z_1}^{z_1{}'}\frac{dz}{\sigma'} \Rightarrow$$

$$R_{c_1} = \frac{l}{\sigma_0}\left[1 - exp\left(-\frac{z_c - d/2}{l}\right)\right] + \frac{nl}{\sigma_0}\left[exp\left(-\frac{z_c - d/2}{l}\right) - exp\left(-\frac{z_{c_1} - d_1/2}{l}\right)\right] \tag{15}$$

And again, from Ohm's law and equation (15), we get the electric field at ground level for the case of a charged cylindrical monopole as:

$$E_{z_0,Q} = \frac{V_A}{l\left[1 - exp\left(-\frac{z_c - d/2}{l}\right)\right] + nl\left[exp\left(-\frac{z_c - d/2}{l}\right) - exp\left(-\frac{z_{c_1} - d_1/2}{l}\right)\right]} \tag{16}$$

with $E_{z_0,Q}$ being dependent on the scale height l, the conductivity reduction factor n, the central layer height z_c and the charged

255   area central height z_{c_1}.

In the case of multiple stratified charged areas within the layer, the electric field at ground level is a superposition of the contribution to the field from each charge and its image (E_{z_0,Q_i}), along with the non-stratified dust layer's contribution attributed to the imposed conductivity reduction ($E_{z_0,layer}$), hence:

$$E_{z_0,multipole} = \sum E_{z_0,Q_i} + E_{z_0,layer} \Rightarrow$$
$$E_{z_0,dipole} = E_{z_0,\text{lower cylinder}} + E_{z_0,\text{upper cylinder}} + E_{z_0,layer} \tag{17}$$

3 Results

260   In this section, the near ground electric field measurements with co-located lidar observations are presented for the four case studies of elevated Saharan dust layers, over the two atmospheric remote sensing stations. The transient dust events recorded by Polly^{XT} were electrically monitored throughout the day with the field mill.

The July 2017 and March 2018 dust events in Finokalia are characterized by large concentrations of airborne dust particles from the middle of the day onwards, with low near surface concentrations of both dust and marine aerosols, followed by

265   advection towards the ground after 21:00 UTC (Fig. 4 and Fig. 6). In the areas of large total attenuated backscatter, high concentrations are expected and the VLDR values vary from 25% - 35% for both cases, which indicates pure dust areas intermingled with mixed dust. The October 2018 Antikythera layer (Fig. 5), exhibits dust particle concentrations from 2 to 5 km in altitude, mostly mixed with some low marine aerosol concentrations (Fig. 1b). The June 2019 dust outbreak consists primarily of high elevated dust concentrations (Fig. 1d), after mid-day, with pure dust VLDR values reaching up to 40% (Fig.

270   7), while aerosol concentrations within the Planetary Boundary Layer (PBL) are present but the dust load remains dominant between 2 km and 5 km.

As seen in Fig. 4 and Fig. 6, where the LREF and the reconstructed mean electric field are depicted in Finokalia, the local diurnal variation resembles the Carnegie curve. The E_z values vary between a total minimum at ~ 05:00 (UTC) and the maximum at ~ 13:00 (UTC) with a mean value of ~ 173 V/m. An increase of the electric field is observed at about 22:00

275   (UTC) resulting in a double peak variations curve (Yaniv et al., 2016). The reconstructed mean E-field is close to the expected fair weather value and the slight difference can be attributed to local meteorological factors, atmospheric boundary layer

characteristics (Anisimov et al., 2017) and the station's coastal location. Complementarily, E_z diurnal variation in the station of Antikythera exhibits a minimum in early morning hours at ~ 23:00 (UTC) and a single maximum on early afternoon at ~ 19:00 (UTC) (Fig. 5 and Fig. 7), with a mean value of ~ 102 V/m. Since the timeseries in Antikythera are restricted to one
280   year, the mean E_z value is statistically biased, therefore it is lower than the expected fair weather value.

According to the effect over the E-field timeseries, the dust outbreaks examined here are separated into two classes, the ones that effectuate an enhancement to the ground electric field and those inducing a reduction with respect to the local reference field.

3.1 Observed E-Field enhancement as compared to LREF

285   The cases with enhanced electrical behaviour at the surface are presented in Fig. 4 and Fig. 5. In the July 25th layer (Fig. 4), dust advection is recorded during the first morning hours and areas of increased particle concentration can be spotted from early noon, as indicated by the total attenuated backscatter coefficient dependence from the altitude. Larger particle concentrations are shown in red tones (Fig. 4). The VLDR values for the same dust layer are also plotted on the lower panel and signify that the layer consists primarily of dust which descends after ~16:00 UTC and falls entirely below 2 km at ~18:30
290   UTC. The E-field measurements are averaged over 5 mins in order to be plotted against the lidar data and remain consistently above the LREF, showing an increase when particle density is maximized towards noon and a small drop when dust concentrations within the PBL become significant.

A similar electrical behaviour was observed during the dust event of October 2018 that reached the PANGEA observatory. Large lofted particle concentrations are attributed to dust according to VLDR values that reach up to 30% (Fig. 5). It is also
295   observed that the near-ground dust concentration is very low, with the thin layer at 500 m being of marine origin. For both cases, the mean E_z appears enhanced as compared to the reference field.

3.2 Observed E-Field reduction as compared to LREF

Several dust load cases were detected, both in Finokalia and Antikythera, where the near-ground electric field exhibits a decrease when compared to the local reference field and, particularly, when high dust particle concentrations were present. In
300   the specific study, we select the cases of March 2018 and June 2019 in terms of the similar injection of dust particles, large AOD values and similar layer progression throughout the day. As observed in Fig. 6, an elevated layer with no dust concentrations near the surface reached Finokalia in March 14th 2018, at early noon. The layer was directly transported from Sahara and reached the station in less than 48 hours as indicated by the backward trajectories analysis (Fig. 1c). From the VLDR values (35% - 40%), we deduce that the layer consists mainly of pure dust which remains elevated between 1.5 and 4
305   km. The mean E-field remains positive and well below the reference field, exhibiting an increase as dust injection initiates at ~11:00 UTC and then a decrease along the plume's progression (Fig. 6).

The dust plume of June 2019 was transported again directly from Sahara to Antikythera within 48 hours (Fig. 1d), while PBL particle concentrations were high over early morning hours and decreased as the elevated dust particle densities increase near

noon. A daily average AOD value of 0.22 indicates that there is high concentration of aerosols throughout the day and the
310 VLDR values attained from the lidar, peak to as high as 40% in the height of 4 km within the layer (Fig. 7). Dust seems to
progressively move downwards during late afternoon but the dust load is persistent and renewed in the following day.
Moreover, the effect of the dust plume on the electric field is clearly similar to the previous case in Finokalia, where the mean
field remains positive and always below the LREF but appears to be increasing with rising dust concentrations.

315 Through observations of the electric field during the dust outbreaks reported above, we can attempt to provide evidence of
electrically active dust by ground-based methods. In order to explain the observed electrical behaviour, we examine the ground
E-field effect of electrically neutral dust at first and thereafter calculate the E-field strength following the formalism for a
charge stratified dust layer (see Section 2.3). Then, we compare it with the E-field values under local fair weather conditions
for selected atmospheric electric parameters. Following this formulation, the dust layer that exhibits charge separation is
320 approximated with a dipole of oppositely charged cylinders. If multiple charge accumulation regions are suspected, the
problem can be represented by a superposition of several cylindrical monopoles with different charge densities, polarities and
separation distances. In section 3.3.3 we also investigate the influence of small charge imbalances (less than 10%) in the bipolar
case, which could quantitatively explain the enhancement and reduction in the E-field.

3.3 Modelled E-field below the LREF

325 In this section, we describe the possible cases under which lofted dust layers can reduce the near-ground electric field strength
below the reference electric field values, and investigate whether electrified dust layers can reproduce such a behaviour. Since
there is little data on the profiling of the electrical properties of elevated dust layers and, to this point, there is no clear depiction
of the potential charge accumulations areas, we use the previous measurements of electric field change with altitude, which
indicated a charge density of $\rho = \pm\ 25$ pC/m^3 within a transported Saharan dust layer away from the emission source (Nicoll
330 et al., 2011). From the specific value, the total charge Q is estimated for the different model cylinder extents. In order to
calculate E_{z_0}, $E_{z_0,layer}$ and $E_{z_0,Q}$, the scale height is fixed to a globally average value of $l = 6$ km (Kalinin et al., 2014;
Stolzenburg and Marshall, 2008), the ionospheric potential is fixed at $V_{ion} = 250$ kV and the ionospheric height is at $H = 70$
km. The mean central height of the dust layer and mean layer depth are both set equal to 3 km ($z_c = 3$ km, $d = 3$), since this
height represents the average value for the four dust cases according to the lidar VLDR profiles (Table 1).

335 3.3.1 Dust layer acting as a passive element

In Fig. 8., the dependence of $E_{z_0,layer}$ (red line) on the conductivity reduction factor, the scale height, the layer central height
and the layer depth, as given in (11), is plotted and compared to the fair weather electric field E_{z_0} at ground (blue line) which
is given by (7). E_{z_0} depends only on the scale height and decreases as l increases, while it remains constant for the other
varying parameters as expected from equation (7). The calculated fair weather field value of ~ 42 V/m, for the selected l, is
340 comparable to the estimated value by Williams (2003) from Ohm's law, when dividing the globally integrated conduction

current density by the mean atmospheric electrical conductivity at ground ($J_{z_0} \approx 2x10^{-12} A/m^2, \sigma_0 \approx 5x10^{-14} S/m$) and assuming an exponentially increasing conductivity profile above the Earth's surface (Haldoupis et al., 2017). We note that this globally average value of E_{z_0} is much less from the typically measured which is around 100 V/m (e.g. Corney et al., 2003; Reddell et al., 2004). We believe that the average value is more suitable for global calculations, because it incorporates the

345   variations of the conductivity distribution around the Earth. On the other hand, the typical value is tied to the location of the measurement, and it varies at different locations as the conductivity distribution changes.

Consequently, $E_{z_0,layer}$ exhibits the greatest variation with the reduction factor n, meaning that atmospheric conductivity reduction is the predominant factor that affects the E-field strength by largely lowering it. Therefore, we expect that if the dust layer is electrically neutral, it reduces the atmospheric conductivity and affects the ground electric field by forcing it below the

350   local reference values. Gringel and Muhleisen (1978) measured a reduction of the electrical conductivity, compared to the fair weather values, by a factor of four within an elevated dust layer, while an increase of the electric field within an Alpine peak layer by a factor of two has also been observed (Reiter, 1992). We, therefore, adopt a reduction factor of $n = 4$ in the present study.

3.3.2 Balanced charged dipole field below the LREF

355   We consider the case of two oppositely charged cylinders with similar geometries as in Fig. 3c, assuming they are within a dust layer with a mean height of 3 km and a mean depth of 3 km. The lower cylinder central height z_{c_1} starts at 2.95 km and decreases, the upper cylinder central height z_{c_2} starts also at 2.95 km for zero separation distance (at this limit, it represents electrically neutral dust that lacks internal E-field generation due to the absence of charge separation) and increases within the dust layer boundaries (varying separation distance), while their depth is fixed at 100 m. The separation distance between the

360   two cylinders is defined as the difference between their central heights and the ground E-field is a superposition of the electric field of the upper and lower cylinders. We assume the bottom cylinder to be positively charged with density $+\rho$ and the upper one to be negatively charged with $-\rho$, in order to simulate gravitational settling conditions for larger and, most probably, positively charged dust particles (Forward et al., 2009; Waitukaitis et al., 2014).

From equations (12) to (17), the field is analytically calculated directly on the axis of the charged cylinders and plotted against

365   the cylinder radius R for separation distances up to 800 m (Fig. 9). As seen in Fig. 9, the resulting electric field values on ground level are consistently below the fair weather constant value. When the dipole separation distance increases, the vertical electric field at ground level increases, but when kept relatively small (Fig. 9), the E-field increases but not sufficiently to overcome the LREF. This happens due to the fact that as the upper charged layer moves to higher altitudes, the resistance between the layer and the ground increases, therefore the conduction current at the ground decreases. Hence, the conduction

370   current due to the upper charged layer is weaker than the conduction current due to the lower charged layer, which moves towards the ground. Since the conductivity at the ground is undisturbed by the layer and equal to the fair weather value, the ground electric field due to the upper layer decreases as the layer moves up, while the field due to the lower layer increases as the layer approaches the ground, leading to an increasing value of the total electric field with the increasing separation distance.

For large radii, although the infinite plates configuration is asymptotically approached ($E_{z_0,dipole} \rightarrow 0$), there is a nearly-

375   constant residual field for the finite cylindrical geometry of the charged regions. Since the charged cylinders are placed in a conducting medium above a perfect conductor, the electric field at the ground will not be zero even if the cylinders have infinite extent. Due to the conductivity distribution, there is an uneven contribution of the electric fields of each cylinder and, therefore, the E-field is expected to converge to this non-zero value (Fig. 9).

3.3.3 Imbalanced charged dipole field below the LREF

380   If we assume that the dipole charge density is not uniformly distributed to both cylinders, leading to a charge imbalance within the layer, we expect that the electric field will be more sensitive to separation distance changes. Such imbalance could be the result of (a) dust charging at the source, prior to any charge separation that may occur (Ette, 1971; Kamra, 1972), (b) charging due to atmospheric current, or (c) charge loss through dry deposition in the PBL. The latter effect may occur when the base dust layer descends into the PBL, as in the case of the June 23rd dust layer. In Fig. 10, the ground electric field dependence on

385   the separation distance and cylinder radius is depicted, for a charge density difference of $\Delta\rho = 2$ pC/m^3 between the two charged cylindrical areas, with the upper one being less charged. This leads to a larger increase of the E-field than in the balanced dipole case, as the effect of the upper cylinder not only decreases as it moves to higher altitudes, but it is also reduced due to the reduction of the total charge density which influences proportionally the electric field. Nevertheless, for relatively small separation distances the resulting field values fall below the LREF values. Therefore, considering an electrically active

390   dust layer that exhibits charge imbalance of less than 10%, can be adequate to interpret the observed reduction of the E-field below the LREF. Note that even a small imbalance can highly increase the external field.

3.4 Modelled E-field above the LREF

We examine the physical arrangement within the dust layer that can provide an enhancement to the electric field above the local reference field, as is the case for the dust outbreaks in the 25th of July and 20th of October.

395   ### 3.4.1 Balanced charge dipole field above the LREF

For the same charged region geometries as in the previous section, we impose larger separation distances for the balanced dipole case, but we strictly remain within the base dust layer mean dimensions. Fig. 11 shows that as the separation distance between the oppositely charged layers increases, an enhancement of the E-field above the local reference values occurs. This enhancement becomes more prominent as the layers grow further apart within the dust plume and the contribution from the

400   lower layer is significantly larger than the upper layer. The above dependence of the ground E-field on the separation distance is not expected in the case of charged infinite plates, as discussed in section 3.3.2. Since the charged cylinders are placed in a conducting medium above a conducting plane, the electric field at the ground is not expected to be zero even if the cylinders have infinite extent. The reason is that at each point of the domain, because of the conductivity distribution, there is an uneven

contribution of the electric fields of each cylinder. Therefore, it is expected at infinite radii of the cylindrical formalism that

405   the field converges to a non-zero value (residual field).

3.4.2 Imbalanced charged dipole field above the LREF

Again, for a charge imbalance of 8% between the two cylinders and for larger separation distances, the E-field is significantly enhanced and exceeds the local fair weather values (Fig. 12). The term large or small separation distance depends on the conductivity distribution and more specifically on the conductivity scale height, as can be seen in equations (11) and (16). This

410   increase becomes more prominent as the separation distance increases and the lower positive cylinder moves closer to the field mill. We also observe that the external E-field is more sensitive to charge imbalance, even a small one, than to separation distance variations, hence when the imbalance is larger than 8% the E-field will exceed the LREF for even smaller separation distances than the ones presented here.

3.4.3 E-field dependence on the bottom charged area height

415   From the above discussion, the question that arises is whether the proximity of the lower cylinder, to the ground itself, is capable to reproduce the electric field enhancement feature above the LREF. It becomes clear that two mechanisms act upon the enhancement of the ground electric field. The first is the decrease of the contribution of the upper layer as it moves upwards, due to the enhancement of the columnar resistance between the layer and the ground. The second is the increase of the contribution of the lower layer as it moves downwards, due to the decrease of the columnar resistance between the layer and

420   the ground. The closer the lower layer is to the ground the smaller the separation with the upper layer is required for the enhancement of the electric field.

In order to validate the influence of each parameter, we re-examine the ground E-field behaviour by keeping the lower cylinder at a fixed altitude of 2 km (close to the dust layer base, similarly to thundercloud activity e.g. Mallios & Pasko, 2012) and we, then, increase the separation distance. As observed in Fig. 13, the increasing separation distance causes the E-field to increase

425   at the ground and when it becomes large enough (Fig. 13, top and bottom right panels), the upper cylinder does no longer influence the ground E-field. At this point, for both balanced and imbalanced dipoles with cylinder radius larger than ~40 km, the field converges to a constant value. This becomes clearer when comparing Fig. 13 with Fig. 9. When the separation distance is 400 m, the electric field at the ground is larger than the reference field in the case of Fig. 13, while at Fig. 9, separation distance equal to 400 m happens when the bottom layer is at 2.75 km. In this case, the field is lower than the reference value

430   which indicates that the closer the bottom layer is to the ground, the smaller the separation distance needed for the enhancement of the ground electric field above the reference field. Moreover, the E-field value for zero separation distance is consistently below the calculated fair weather value. As such, observations of enhanced E-field above the fair weather values, for dust driven days, can be reproduced only when an electrically active dust layer is transported above the fieldmill.

If we assume that the bottom charged area is close to the lofted layer base, we would expect an increase to the ground electric

435   field as the layer progressively moves towards lower altitudes. For the comparison of the E-field timeseries with the descending

layer base (Fig. 14), we use the cross component of the lidar attenuated backscatter coefficient at 532 nm, from which we can derive information on the vertical extent of the aerosol layers. More specifically, we applied a methodology where the first derivative of the attenuated backscatter coefficient is used to determine layer boundaries (Flamant et al., 1997; Mattis et al., 2008). The local maximum and local minimum of the derivative are considered to be the bottom and top of the layer

440 respectively. The agreement between the height time displays of the attenuated backscatter coefficient and the corresponding gradient (Fig. 4 to Fig. 7and Fig. 14) can be used to verify the results of the gradient method.

As seen in the July 2017, March 2018 and June 2019 dust events, there is an enhancement of the reconstructed mean E-field followed by the layer base progression towards the ground, for specific timeframes within the day. This could signify the presence of positive charges accumulated to the layer base.

445 **3.5 Reversed E-field polarity**

If a reversed polarity E-field is observed (in our timeseries there were dust cases under which the field exhibited polarity reversal), with the opposite sign signifying that the field vector points upwards instead of downwards, then the investigated formalism is capable of explaining the reversal. As such, a similar cylindrical configuration is assumed with the only difference being that the lower layer has to be negatively charged and the upper one, in the dipole case, to be positively charged. Under

450 this condition, the conclusions in Fig. 9 to Fig. 12 remain the same. Therefore, such an indication of reversal is explained only via reversed separated cylindrical charges and again points that lofted dust has to be electrified.

4 Discussion

4.1 Chauvenet criterion validity

In section 2.2.2, we described the processing chain for the determination of the local fair weather days at both atmospheric

455 remote sensing stations. The novelty of the approach lies to the fact that only signal processing constraints are used, without incorporating criteria of local meteorological parameters that could redefine the initial conditions for the total fair weather days determination (Harrison & Nicoll, 2018). Nonetheless, threshold values concerning these factors are subjective, and may vary from study to study, which leads to differences in the extracted fair weather days. The specific study proposes a mathematically strict approach with the imposition of the Chauvenet criterion, which exploits only the field mill data and has a physical impact

460 on the dataset. Under fair weather days, the mean electric field is approximately constant and the fewer by far dust driven days as captured in both stations, which are about 10% of the days within a typical year for both stations, will not influence significantly the reconstructed mean field value, but will be well beyond the standard deviation. The Chauvenet criterion excludes the days with such high variations as outliers and, therefore, the methodology for the reconstruction of the local reference field is less biased to variations occurring in dust driven days.

4.2 Generalization of the cylindrical model and LREF methodology

The methodology followed for the calculation of the ground electric field can be expanded to the area away from the central axis of the charged cylinders. As the cylinder radius increases and the infinite plate regime is approached, effects due to charged layer edges that induce radial electric field components, do not impact the sensor axis for a larger horizontal extent of the charged layer. This expands the analytical calculation as it becomes valid within a band region further away from the cylinder center. In the small radius regime, the sensor becomes sensitive to edge effects and the edge field can be far stronger than the on-axis field. If we assume that a transient dust layer is transported with a mean wind speed of 10 m/s, then in a period of 2 hrs the edge will be 72 km away from the sensor axis (fast transits), a sufficient distance to not affect the vertical component of the electric field. Although these variations are present on the raw timeseries (observed peak activity in Fig. 4, Fig. 6 and Fig. 7), in the reconstruction of the LREF variations with timescales shorter than 6 hrs are the lower limit to the FFT input and are therefore excluded. This leaves the LREF unbiased to edge effects. Problems might be caused in our analysis in the case of very slowly moving dust layers, that are transported with wind speeds less than 1 m/s. Dust layer edge effects can provide basic information on the layer properties and could be incorporated in our cylindrical layer formalism, but it will be a subject of further investigation in the near future.

5 Summary and Conclusions

Near-ground electric field strength observations during Saharan dust advection over Greece exhibit three distinct responses of enhancement, reduction or sign reversal when compared to local fair weather values. In this paper, we present four cases of transient dust events that influence the ground electric field recorded at two atmospheric remote sensing stations synergistically with a lidar system and a field mill electrometer. Moreover, this work attempts to use only ground-based atmospheric electricity instrumentation as a proxy for electrified dust detection, with characterization in terms of optical properties from lidar observations. To quantify the effect of charged dust particles, we implemented a reference electric field representing the local fair weather field, using long-term measured timeseries, and examine the possible physical mechanisms that could explain the electric field behaviour. Our findings suggest that dust cases with the reconstructed mean E-field magnitude above the reference field indicate charge separation within the layer either as a balanced or imbalanced dipole (or a multipole) of charge layers, while when the mean field is completely below the reference field, dust electrical activity characterization is inconclusive. This ground electric field reduction below the local fair weather field can be attributed to either the conductivity reduction due to dust acting as a passive neutral element, where the greater the conductivity reduction the lesser the electric field reduction, or to charge separation between areas of accumulated charge.

The electrified dust scheme is approximated either via the absence of dust charge separation or with thin cylindrical finite charge geometries (as opposed to infinite plate analogues) that allow explaining the electric field dependence on the layer height and the separation distance between the regions of charge accumulation. Both concepts have been suggested to explain the observed E-field responses at ground. However, there is no observational evidence up to now to validate the charge strata

Atmospheric
Chemistry
and Physics
Discussions

morphology, which might be far from similar to the elevated layers morphology due to the charged dust particles complex transport dynamics. To constrain the modelling formalism proposed here, future research will include profiling of the columnar electrical properties of dust, deploying airborne platforms (balloons and UAVs) within the Saharan Air Layer during foreseen

500   future experiments at Cyprus and Cape Verde within the years 2020 and 2021.

510

520

Conflicts of Interest: The authors declare no conflict of interest.

References

Anisimov, S. V., Galichenko, S. V. and Mareev, E. A.: Electrodynamic properties and height of atmospheric convective
525 boundary layer, Atmos. Res., 194, 119–129, doi:10.1016/j.atmosres.2017.04.012, 2017.

Bailey, J., Ulanowski, Z., Lucas, P. W., Hough, J. H., Hirst, E. and Tamura, M.: The effect of airborne dust on astronomical
polarization measurements, Mon. Not. R. Astron. Soc., 386(2), 1016–1022, doi:10.1111/j.1365-2966.2008.13088.x, 2008.

Baumgaertner, A. J. G., Lucas, G. M., Thayer, J. P. and Mallios, S. A.: On the role of clouds in the fair weather part of the
global electric circuit, Atmos. Chem. Phys., 14(16), 8599–8610, doi:10.5194/acp-14-8599-2014, 2014.

530 Chubb, J.: The measurement of atmospheric electric fields using pole mounted electrostatic fieldmeters, J. Electrostat., 72(4),
295–300, doi:10.1016/j.elstat.2014.05.002, 2014.

Chubb, J.: Comparison of atmospheric electric field measurements by a pole mounted fieldmeter and by a horizontal wire
antenna, J. Electrostat., 73, 1–5, doi:10.1016/j.elstat.2014.10.003, 2015.

Corney, R. C., Burns, G. B., Michael, K., Frank-Kamenetsky, A. V., Troshichev, O. A., Bering, E. A., Papitashvili, V. O.,
535 Breed, A. M. and Duldig, M. L.: The influence of polar-cap convection on the geoelectric field at Vostok, Antarctica, J. Atmos.
Solar-Terrestrial Phys., 65(3), 345–354, doi:10.1016/S1364-6826(02)00225-0, 2003.

van der Does, M., Knippertz, P., Zschenderlein, P., Giles Harrison, R. and Stuut, J. B. W.: The mysterious long-range transport
of giant mineral dust particles, Sci. Adv., 4(12), 1–9, doi:10.1126/sciadv.aau2768, 2018.

Duff, N. and Lacks, D. J.: Particle dynamics simulations of triboelectric charging in granular insulator systems, J. Electrostat.,
540 66(1–2), 51–57, doi:10.1016/j.elstat.2007.08.005, 2008.

Engelmann, R., Kanitz, T., Baars, H., Heese, B., Althausen, D., Skupin, A., Wandinger, U., Komppula, M., Stachlewska, I. S.,
Amiridis, V., Marinou, E., Mattis, I., Linné, H. and Ansmann, A.: The automated multiwavelength Raman polarization and
water-vapor lidar PollyXT: The neXT generation, Atmos. Meas. Tech., 9(4), 1767–1784, doi:10.5194/amt-9-1767-2016, 2016.

Esposito, F., Molinaro, R., Popa, C. I., Molfese, C., Cozzolino, F., Marty, L., Taj-Eddine, K., Di Achille, G., Franzese, G.,
545 Silvestro, S. and Ori, G. G.: The role of the atmospheric electric field in the dust-lifting process, Geophys. Res. Lett., 43(10),
5501–5508, doi:10.1002/2016GL068463, 2016.

Ette, A. I. I.: The effect of the Harmattan dust on atmospheric electric parameters, J. Atmos. Terr. Phys., 33(2), 295–300,
doi:10.1016/0021-9169(71)90208-X, 1971.

Flamant, C., Pelon, J., Flamant, P. H. and Durand, P.: Lidar determination of the entrainment zone thickness at the top of the
550 unstable marine atmospheric boundary layer, Boundary-Layer Meteorol., 83(2), 247–284, doi:10.1023/A:1000258318944,
1997.

Forward, K. M., Lacks, D. J. and Mohan Sankaran, R.: Particle-size dependent bipolar charging of Martian regolith simulant,
Geophys. Res. Lett., 36(13), 1–5, doi:10.1029/2009GL038589, 2009.

Freier G. D.: The Electric Field of a Large Dust Devil, October, (10), 1960–1960, 1960.

555 Freudenthaler, V., Esselborn, M., Wiegner, M., Heese, B., Tesche, M., Ansmann, A., Müller, D., Althausen, D., Wirth, M.,
Fix, A., Ehret, G., Knippertz, P., Toledano, C., Gasteiger, J., Garhammer, M. and Seefeldner, M.: Depolarization ratio profiling

Atmospheric
Chemistry
and Physics
Discussions
Open Access
EGU

at several wavelengths in pure Saharan dust during SAMUM 2006, Tellus, Ser. B Chem. Phys. Meteorol., 61(1), 165–179, doi:10.1111/j.1600-0889.2008.00396.x, 2009.

Fuchs, N. A.: On the stationary charge distribution on aerosol particles in a bipolar ionic atmosphere, Geofis. Pura e Appl.,

560   56(1), 185–193, doi:10.1007/BF01993343, 1963.

Griffiths, D. J.: Introduction to electrodynamics. Instructor's solutions manual, 3rd edition, Upper Saddle River, N.J, 1999.

Gringel W. and Mulheisen R.: Sahara dust concentration in the troposphere over the north Atlantic derived from measurements of air conductivity Beitr. Phys. Atmos. 51 121–8, 1978.

Gringel, W., J. M. Rosen, and D. J. Hoffmann.: Electrical structure from 0 to 30 km, in The Earth Electrical Environment,

565   edited by E. P. Krider and R. G. Robie, pp. 166-182, Nat. Acad. Press, Washington, D.C., 1986.

Gunn, R.: Diffusion Charging of Atmospheric Droplets By Ions, and the Resulting Combination Coefficients, J. Meteorol., 11(5), 339–347, doi:10.1175/1520-0469(1954)011<0339:dcoadb>2.0.co;2, 1954.

Haarig, M., Ansmann, A., Althausen, D., Klepel, A., Groß, S., Freudenthaler, V., Toledano, C., Mamouri, R. E., Farrell, D. A., Prescod, D. A., Marinou, E., Burton, S. P., Gasteiger, J., Engelmann, R. and Baars, H.: Triple-wavelength depolarization-

570   ratio profiling of Saharan dust over Barbados during SALTRACE in 2013 and 2014, Atmos. Chem. Phys., 17(17), 10767–10794, doi:10.5194/acp-17-10767-2017, 2017.

Haldoupis, C., Rycroft, M., Williams, E. and Price, C.: Is the "Earth-ionosphere capacitor" a valid component in the atmospheric global electric circuit?, J. Atmos. Solar-Terrestrial Phys., 164(August), 127–131, doi:10.1016/j.jastp.2017.08.012, 2017.

575   Harrison, R. G.: The Carnegie Curve, Surv. Geophys., 34(2), 209–232, doi:10.1007/s10712-012-9210-2, 2013.

Harrison, R. G. and Ingram, W. J.: Air-earth current measurements at Kew, London, 1909-1979, Atmos. Res., 76(1–4), 49–64, doi:10.1016/j.atmosres.2004.11.022, 2005.

Harrison, R. G. and Nicoll, K. A.: Fair weather criteria for atmospheric electricity measurements, J. Atmos. Solar-Terrestrial Phys., 179(February), 239–250, doi:10.1016/j.jastp.2018.07.008, 2018.

580   Harrison, R. G., Nicoll, K. A., Ulanowski, Z. and Mather, T. A.: Self-charging of the Eyjafjallajökull volcanic ash plume, Environ. Res. Lett., 5(2), 3–7, doi:10.1088/1748-9326/5/2/024004, 2010.

Harrison, R. G., Barth, E., Esposito, F., Merrison, J., Montmessin, F., Aplin, K. L., Borlina, C., Berthelier, J. J., Déprez, G., Farrell, W. M., Houghton, I. M. P., Renno, N. O., Nicoll, K. A., Tripathi, S. N. and Zimmerman, M.: Applications of Electrified Dust and Dust Devil Electrodynamics to Martian Atmospheric Electricity, Space Sci. Rev., 203(1–4), 299–345,

585   doi:10.1007/s11214-016-0241-8, 2016.

Harrison, R. G., Nicoll, K. A., Marlton, G. J., Ryder, C. L. and Bennett, A. J.: Saharan dust plume charging observed over the UK, Environ. Res. Lett., 13(5), doi:10.1088/1748-9326/aabcd9, 2018.

Inculet, I. I., Castle, G. S. P. and Aartsen, G.: Generation of bipolar electric fields during industrial handling of powders, Chem. Eng. Sci., 61(7), 2249–2253, doi:10.1016/j.ces.2005.05.005, 2006.

590   Kalinin, A. V., Slyunyaev, N. N., Mareev, E. A. and Zhidkov, A. A.: Stationary and nonstationary models of the global electric

circuit: Well-posedness, analytical relations, and numerical implementation, Izv. - Atmos. Ocean Phys., 50(3), 314–322, doi:10.1134/S0001433814030074, 2014.

Kamra, a. K.: Measurements of the electrical properties of dust storms, J. Geophys. Res., 77(30), 5856, doi:10.1029/JC077i030p05856, 1972.

595   Kanagy, S. P. and Mann, C. J.: Electrical properties of eolian sand and silt, Earth Sci. Rev., 36(3–4), 181–204, doi:10.1016/0012-8252(94)90057-4, 1994.

Katz, S., Yair, Y., Price, C., Yaniv, R., Silber, I., Lynn, B. and Ziv, B.: Electrical properties of the 8–12th September, 2015 massive dust outbreak over the Levant, Atmos. Res., 201(November 2017), 218–225, doi:10.1016/j.atmosres.2017.11.004, 2018.

600   Kok, J. F. and Renno, N. O.: Enhancement of the emission of mineral dust aerosols by electric forces, Geophys. Res. Lett., 33(19), 2–6, doi:10.1029/2006gl026284, 2006.

Krehbiel, P. R., Riousset, J. A., Pasko, V. P., Thomas, R. J., Rison, W., Stanley, M. A. and Edens, H. E.: Upward electrical discharges from thunderstorms, Nat. Geosci., 1(4), 233–237, doi:10.1038/ngeo162, 2008.

Lacks, D. J. and Shinbrot, T.: Long-standing and unresolved issues in triboelectric charging, Nat. Rev. Chem., 3(8), 465–476,
605   doi:10.1038/s41570-019-0115-1, 2019.

Lelieveld, J., Berresheim, H., Borrmann, S., Crutzen, P. J., Dentener, F. J., Fischer, H., Feichter, J., Flatau, P. J., Heland, J., Holzinger, R., Korrmann, R., Lawrence, M. G., Levin, Z., Markowicz, K. M., Mihalopoulos, N., Minikin, A., Ramanathan, V., De Reus, M., Roelofs, G. J., Scheeren, H. A., Sciare, J., Schlager, H., Schultz, M., Siegmund, P., Steil, B., Stephanou, E. G., Stier, P., Traub, M., Warneke, C., Williams, J. and Ziereis, H.: Global air pollution crossroads over the Mediterranean,
610   Science (80-.)., 298(5594), 794–799, doi:10.1126/science.1075457, 2002.

Mallios, S. A. and Pasko, V. P.: Charge transfer to the ionosphere and to the ground during thunderstorms, J. Geophys. Res. Sp. Phys., 117(8), 1–16, doi:10.1029/2011JA017061, 2012.

Mattis, I., Müller, D., Ansmann, A., Wandinger, U., Preißler, J., Seifert, P. and Tesche, M.: Ten years of multiwavelength Raman lidar observations of free-tropospheric aerosol layers over central Europe: Geometrical properties and annual cycle, J.
615   Geophys. Res. Atmos., 113(20), 1–19, doi:10.1029/2007JD009636, 2008.

Nicoll, K. A., Harrison, R. G. and Ulanowski, Z.: Observations of Saharan dust layer electrification, Environ. Res. Lett., 6(1), 1–8, doi:10.1088/1748-9326/6/1/014001, 2011.

Rakov V. A., & Uman M. A. Lightning: Physics and Effects , Cambridge U. Press, New York, 2003.

Reddell, B. D., Benbrook, J. R., Bering, E. A., Cleary, E. N. and Few, A. A.: Seasonal variations of atmospheric electricity
620   measured at Amundsen-Scott South Pole Station, J. Geophys. Res. Sp. Phys., 109(A9), 1–17, doi:10.1029/2004JA010536, 2004.

Renno, N. O. and Kok, J. F.: Electrical activity and dust lifting on earth, Mars, and beyond, Space Sci. Rev., 137(1–4), 419–434, doi:10.1007/s11214-008-9377-5, 2008.

Riousset, J. A., Pasko, V. P., Krehbiel, P. R., Thomas, R. J. and Rison, W.: Three-dimensional fractal modeling of intracloud

625 lightning discharge in a New Mexico thunderstorm and comparison with lightning mapping observations, J. Geophys. Res. Atmos., 112(15), 1–17, doi:10.1029/2006JD007621, 2007.

Rycroft, M. J., Harrison, R. G., Nicoll, K. A. and Mareev, E. A.: An overview of earth's global electric circuit and atmospheric conductivity, Space Sci. Rev., 137(1–4), 83–105, doi:10.1007/s11214-008-9368-6, 2008.

Ryder, C. L., Marenco, F., Brooke, J. K., Estelles, V., Cotton, R., Formenti, P., McQuaid, J. B., Price, H. C., Liu, D., Ausset,
630 P., Rosenberg, P., Taylor, J. W., Choularton, T., Bower, K., Coe, H., Gallagher, M., Crosier, J., Lloyd, G., Highwood, E. J. and Murray, B. J.: Coarse mode mineral dust size distributions, composition and optical properties from AER-D aircraft measurements over the Tropical Eastern Atlantic, Atmos. Chem. Phys. Discuss., 98, 1–49, doi:10.5194/acp-2018-739, 2018.

Silva, H. G., Lopes, F. M., Pereira, S., Nicoll, K., Barbosa, S. M., Conceição, R., Neves, S., Harrison, R. G. and Collares Pereira, M.: Saharan dust electrification perceived by a triangle of atmospheric electricity stations in Southern Portugal, J.
635 Electrostat., 84, 106–120, doi:10.1016/j.elstat.2016.10.002, 2016.

Solomos, S., Kalivitis, N., Mihalopoulos, N., Amiridis, V., Kouvarakis, G., Gkikas, A., Binietoglou, I., Tsekeri, A., Kazadzis, S., Kottas, M., Pradhan, Y., Proestakis, E., Nastos, P. T. and Marenco, F.: From tropospheric folding to Khamsin and Foehn winds: How atmospheric dynamics advanced a record-breaking dust episode in Crete, Atmosphere (Basel)., 9(7), doi:10.3390/atmos9070240, 2018.

640 Stolzenburg, M. and Marshall, T. C.: Charge structure and dynamics in thunderstorms, Space Sci. Rev., 137(1–4), 355–372, doi:10.1007/s11214-008-9338-z, 2008.

Tegen, I., Hollrig, P., Chin, M., Fung, I., Jacob, D. and Penner, J.: Contribution of different aerosol species to the global aerosol extinction optical thickness: Estimates from model results, J. Geophys. Res. Atmos., 102(20), 23895–23915, doi:10.1029/97jd01864, 1997.

645 Tinsley, B. A. and Zhou, L.: Initial results of a global circuit model with variable stratospheric and tropospheric aerosols, , 111(August), 1–23, doi:10.1029/2005JD006988, 2006.

Ulanowski, Z., Bailey, J., Lucas, P., Hough, J. and Hirst, E.: Alighnment of atmospheric mineral dust due to electric field, Atmos. Chem. Phys., 7, 6161–6173, 2007.

Waitukaitis, S. R., Lee, V., Pierson, J. M., Forman, S. L. and Jaeger, H. M.: Size-dependent same-material tribocharging in
650 insulating grains, Phys. Rev. Lett., 112(21), 1–5, doi:10.1103/PhysRevLett.112.218001, 2014.

Whitby K. T., Liu B. Y. H.: The electrical behaviour of aerosols, Aerosol Science, C. N. Davies, Ed., Academic Press, 1966.

Williams, E.R.: Global electric circuit. In: Holton, J.R., Pyle, J.A., Curry, J.A. (Eds.), Encyclopedia of Atmospheric Sciences. Academic Press, pp. 724–733, 2003.

Wright, H. L.: The influence of atmospheric suspensoids upon the earth's electric field as indicated by observations at kew
655 observatory, Proc. Phys. Soc., 45(2), 152–171, doi:10.1088/0959-5309/45/2/303, 1933.

Yair, Y., Katz, S., Yaniv, R., Ziv, B. and Price, C.: An electrified dust storm over the Negev desert, Israel, Atmos. Res., 181, 63–71, doi:10.1016/j.atmosres.2016.06.011, 2016.

Yaniv, R., Yair, Y., Price, C. and Katz, S.: Local and global impacts on the fair-weather electric field in Israel, Atmos. Res.,

172–173, 119–125, doi:10.1016/j.atmosres.2015.12.025, 2016.

660   Yaniv, R., Yair, Y., Price, C., Mkrtchyan, H., Lynn, B. and Reymers, A.: Ground-based measurements of the vertical E-field in mountainous regions and the "Austausch" effect, Atmos. Res., 189, 127–133, doi:10.1016/j.atmosres.2017.01.018, 2017.

Zheng, X.-J.: Electrification of wind-blown sand: Recent advances and key issues, Eur. Phys. J. E, 36(12), 138, doi:10.1140/epje/i2013-13138-4, 2013.

665
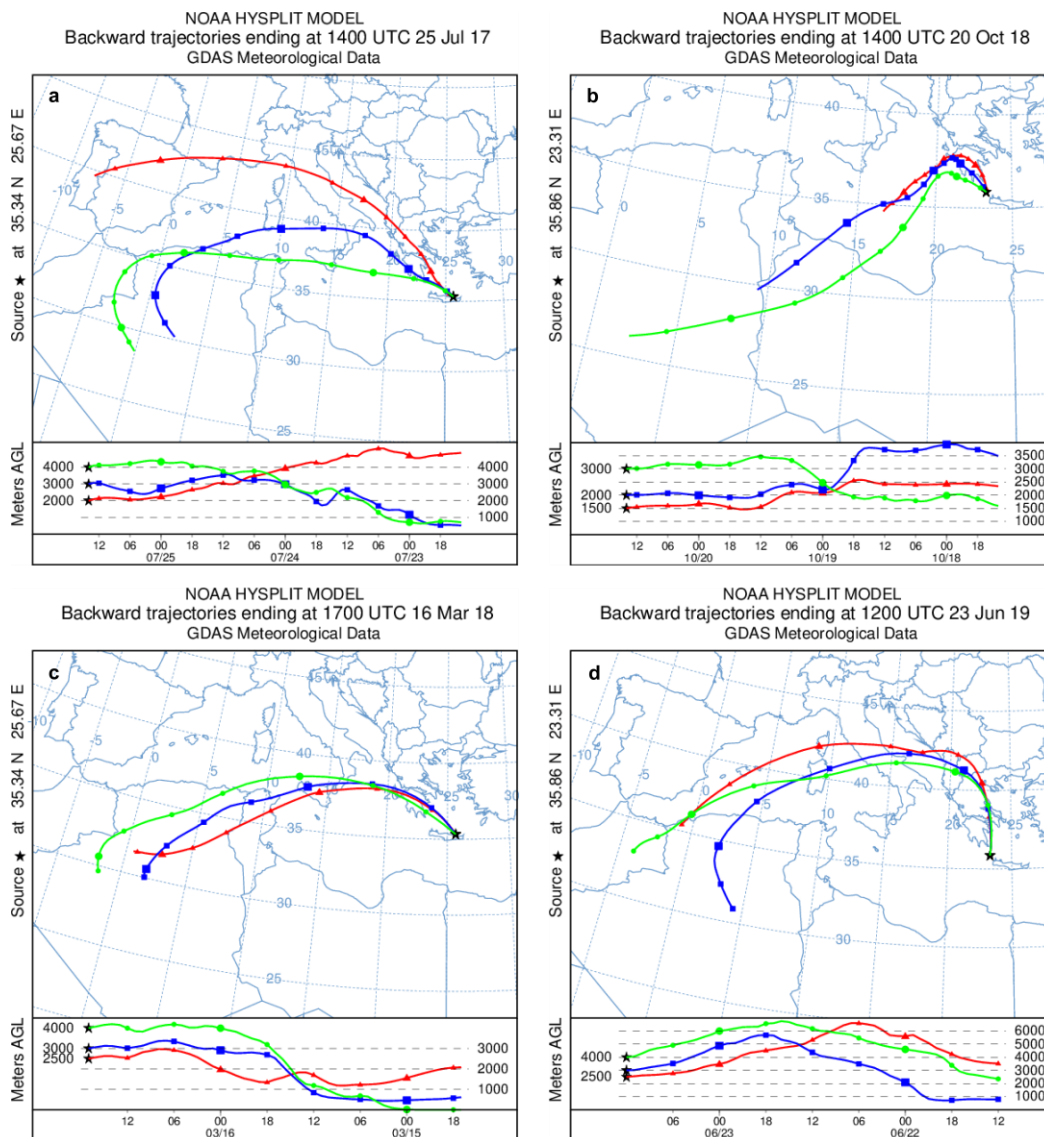
Fig. 1. NOAA HYSPLIT back trajectories for: (a) 25/07/2017 – 72 hrs (Fin.), (b) 20/10/2018 – 72 hrs (Antik.), (c) 16/03/2018 – 48 hrs (Fin.) and (d) 23/06/2019 – 48 hrs (Antik.) backward propagation of air masses.

670

675
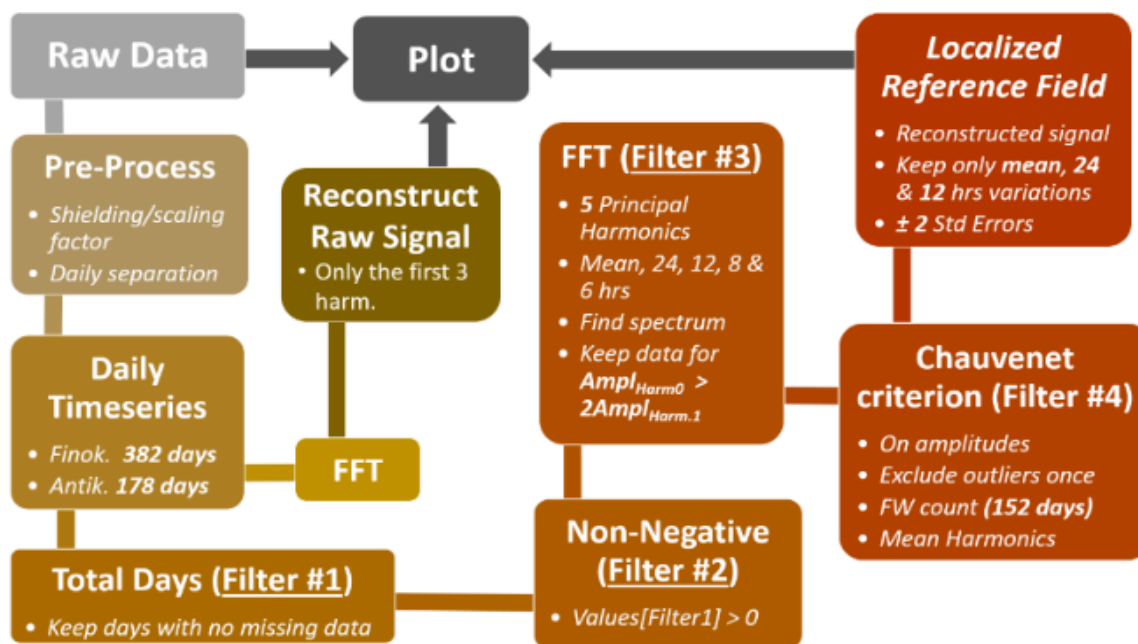
Fig. 2. Signal processing chain for: (i) the derivation of the Localized Reference Electric Field (LREF) that represents the local fair weather conditions and (ii) the derivation of the daily mean electric field under dust driven days. The LREF is compared to the mean electric field values in order to assess the electric field behavior.

Atmospheric
Chemistry
and Physics
Discussions

Open Access

680
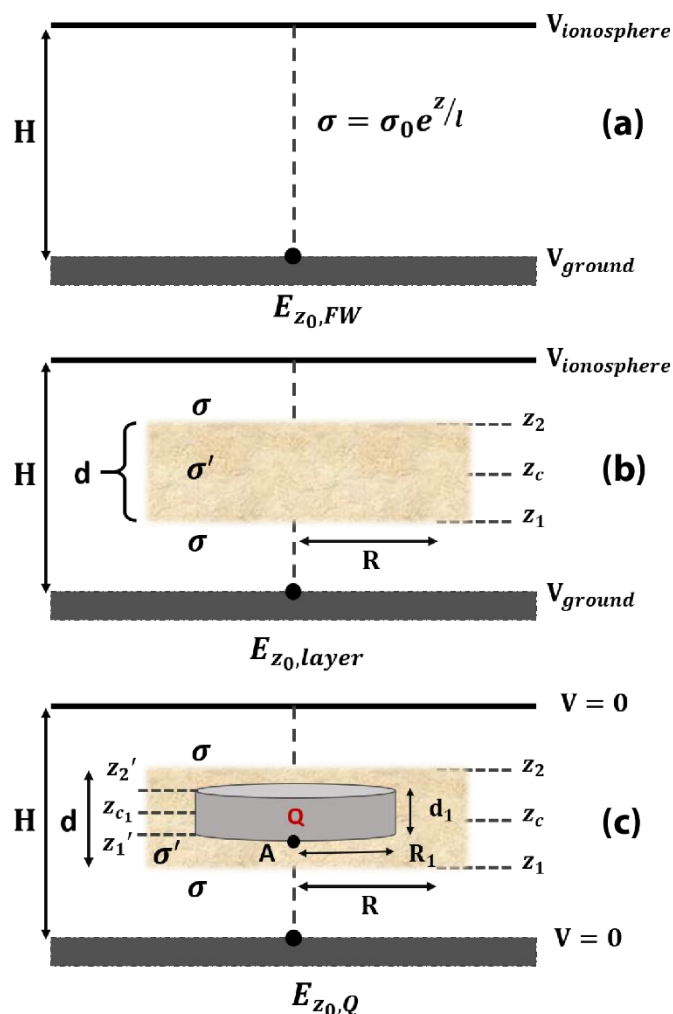
Fig. 3. Schematic of the formalism for the calculation of the steady state surface electric field under: (a) fair weather conditions, (b) the presence of an electrically neutral dust layer which reduces conductivity σ' and (c) the hypothesis of a cylindrical charged monopole within the dust layer. The monopole case is a superposition of the electrically neutral dust layer with the charged cylinder within a bounded atmospheric potential.

690
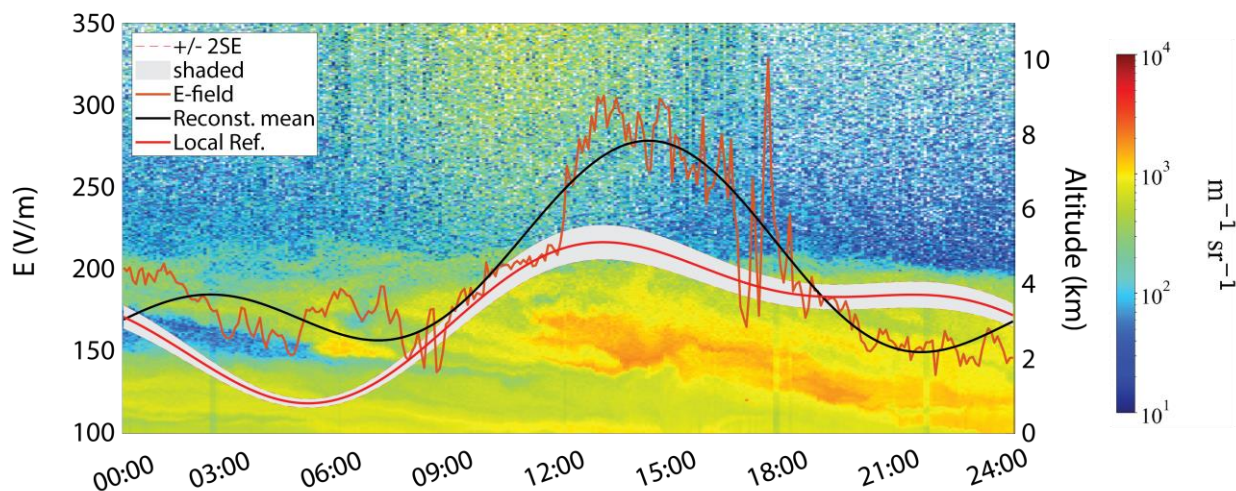
Fig. 4. Top panel: Timeseries of the vertical electric field strength (orange), the Localized Reference Electric Field (red) and the reconstructed mean electric field variation (black) plotted with the Total Attenuated backscatter coefficient against the altitude, for the 25/07/2017 dust layer in Finokalia. Areas of increased particle concentration are denoted with reddish tones. The mean E-field is consistently above the reference field. Bottom panel: Volume Linear Depolarization Ratio (%) for the same dust layer as obtained from the Polly[XT] lidar. VLDR values between 25% and 30% indicate the presence of mostly mixed dust within the layer.

700

Electric Field strength vs Total Attenuated Backscatter coef. at 1064nm - October 20th 2018, Antikythera
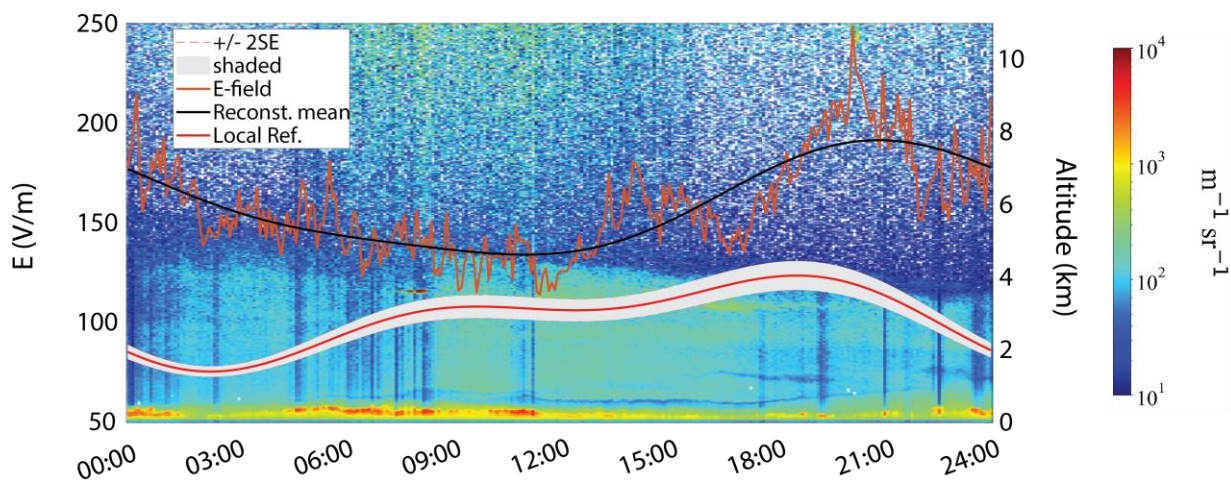
PollyXT Volume Linear Depolarization Ratio at 532nm - October 20th 2018, Antikythera
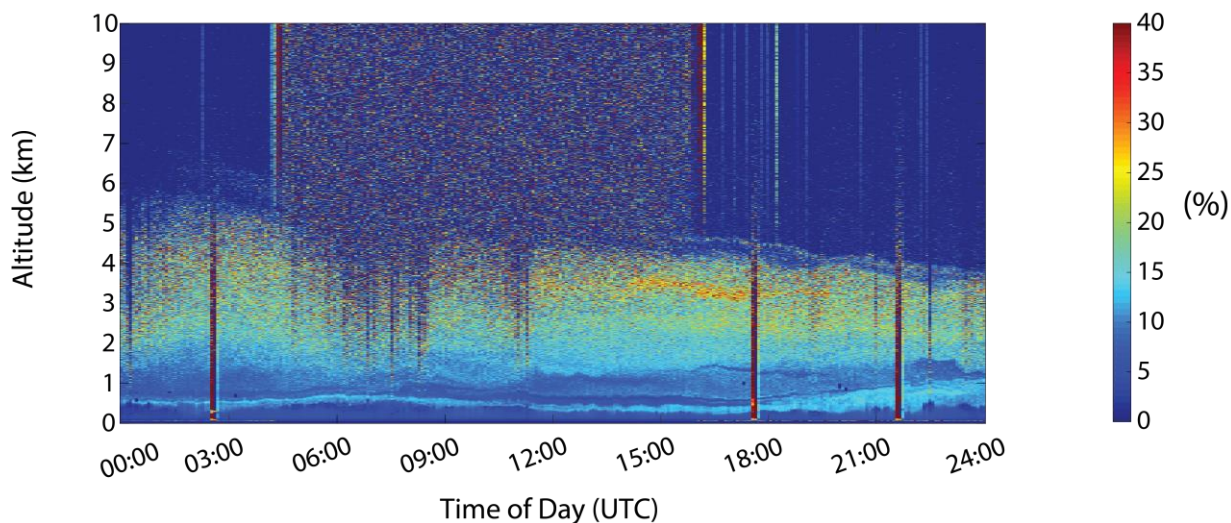
Fig. 5. <u>Top panel</u>: **Timeseries of the vertical electric field strength (orange), the Localized Reference Electric Field (red) and the reconstructed mean electric field variation (black), plotted with the Total Attenuated backscatter coefficient against the altitude, for the 20/10/2018 dust layer in Antikythera. Areas of increased particle concentration are denoted again with reddish tones. The mean E-field is consistently above the reference field, showing an increase at ~2100 UTC, when dust deposition becomes prominent. <u>Bottom panel</u>: Volume Linear Depolarization Ratio (%) for the same dust layer as obtained from the PollyXT lidar. VLDR values between 25% and 30% indicate the presence of mostly mixed dust within the layer.**

705

710

Electric Field strength vs Total Attenuated Backscatter coef. at 1064nm - March 16th 2018, Finokalia
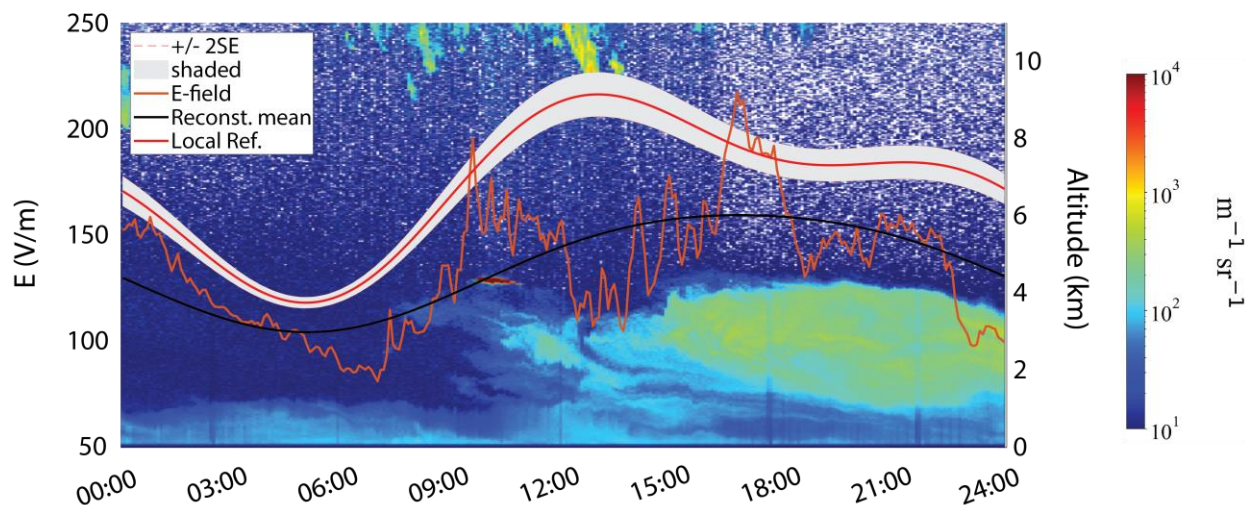
Polly^XT Volume Linear Depolarization Ratio at 532nm - March 16th 2018, Finokalia
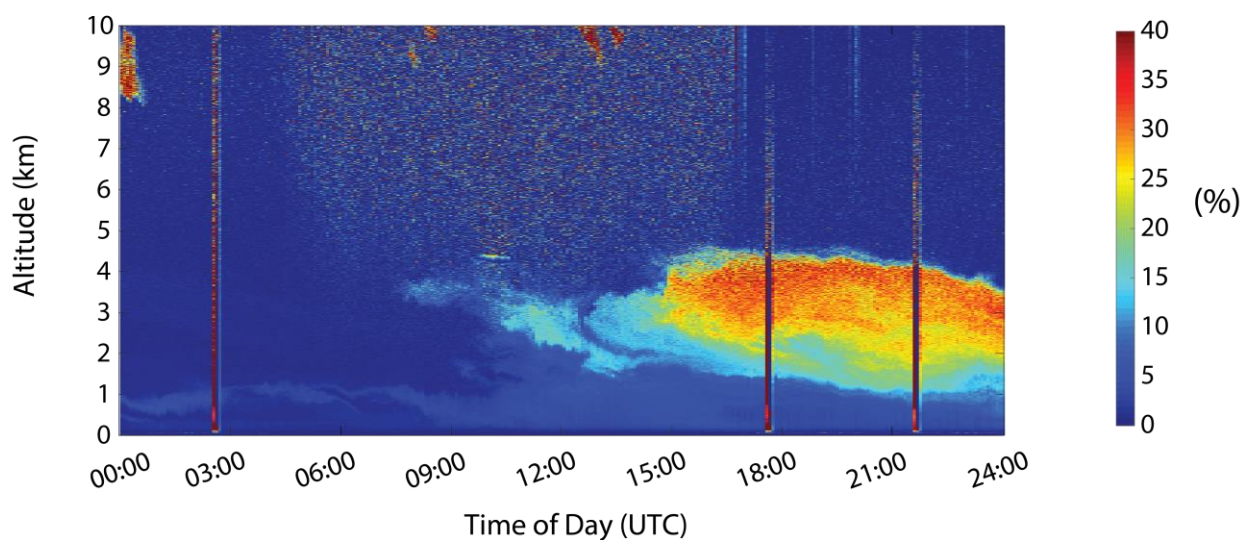
Fig. 6. <u>Top panel</u>: **Timeseries of the vertical electric field strength (orange), the Localized Reference Electric Field (red) and the reconstructed mean electric field variation (black), plotted with the Total Attenuated backscatter coefficient against the altitude, for**
715 **the 16/03/2018 dust layer in Finokalia. Areas of increased particle concentration are denoted with red tones. The mean E-field remains positive and well below the reference field, exhibiting an increase as particle injection initiates at ~1100 UTC and then a decrease along the plume's progression.** <u>Bottom panel</u>: **Volume Linear Depolarization Ratio (%) for the same dust layer as obtained from the Polly^XT lidar. VLDR values between 35% and 40% indicate a pure dust layer within 1.5 km and 4 km, with no surface dust concentration.**

Atmospheric
Chemistry
and Physics
Discussions
Open Access
EGU

720
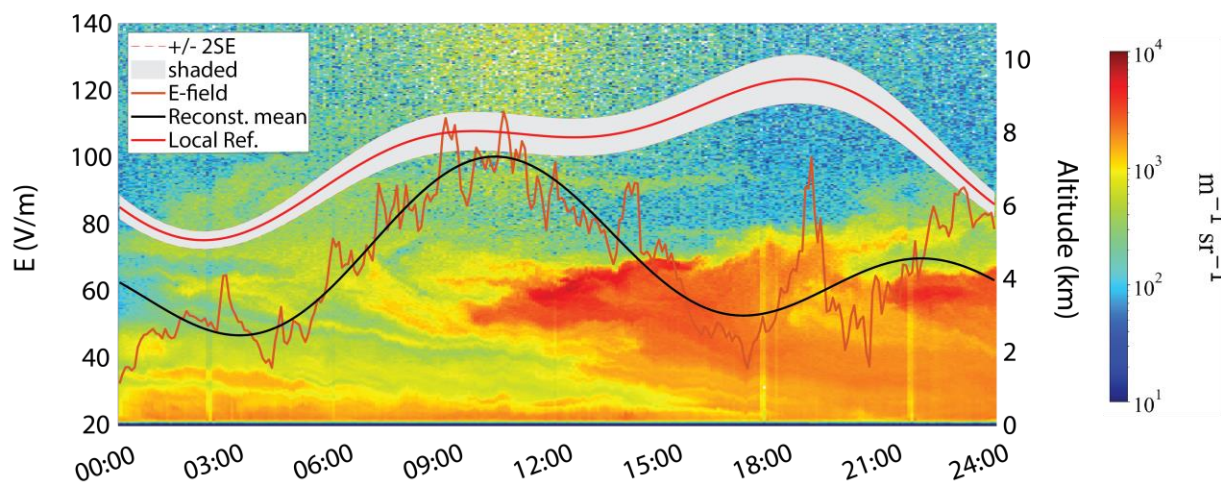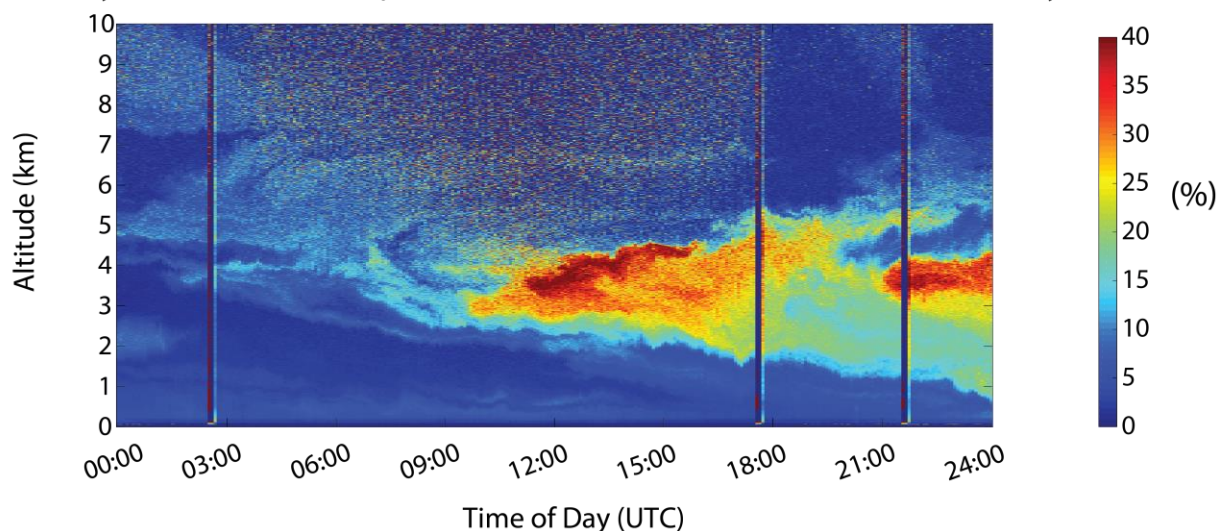
Fig. 7. <u>Top panel</u>: **Timeseries of the vertical electric field strength (orange), the Localized Reference Electric Field (red) and the reconstructed mean electric field variation (black), plotted with the Total Attenuated backscatter coefficient against the altitude, for the 23/06/2019 dust layer in Antikythera. Areas of increased particle concentration are denoted with red tones. The mean E-field is positive and consistently below the reference field, exhibiting an increase when particle injection begins towards noon and further drops as the layer progresses to lower altitudes.** <u>Bottom panel</u>: **Volume Linear Depolarization Ratio (%) for the same dust layer as obtained from the Polly^{XT} lidar. VLDR values between 35% and 40% indicate a pure dust layer within 2 km and 4.5 km, with no surface dust concentration.**

725

730
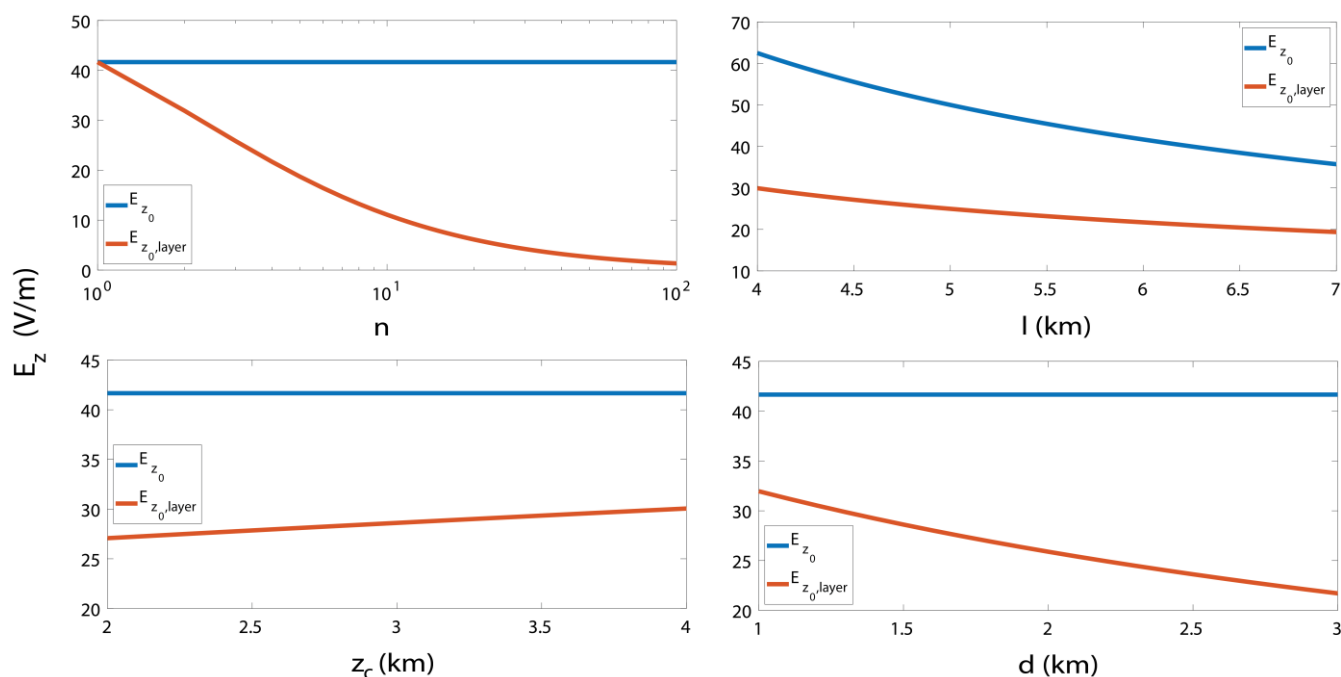
735

Fig. 8. Dependence of the vertical electric field, at ground level, under fair weather (E_{z_0}, blue line) and under the influence of an uncharged dust layer ($E_{z_0,layer}$, red line) on: (a) the reduction factor n, (b) the scaling height l, (c) the central layer height z_c and (d) the separation distance d, for $1/\sigma_0 = 3 \cdot 10^{13} \, \Omega \, m$, $V_{ion} = 250 \, kV$ and $H = 70 \, km$. $E_{z_0,layer}$ strongly depends on the conductivity reduction as depicted in the case (a) curve, where the field reduces with the increasing reduction factor more effectively than with respect to the other three parameters. E_{z_0} depends only on the scaling height as expected.

740

745   **Table 1. Dust layer central height and depth, as derived from the VLDR plots.**

| Dust Outbreak	$z_{c_i} \, (km)$	$d_i \, (km)$
25/07/2017 (Fin.)	3	4
20/10/2018 (Ant.)	3	4
16/03/2018 (Fin.)	3.5	2.5
23/06/2019 (Ant.)	3.5	3

31
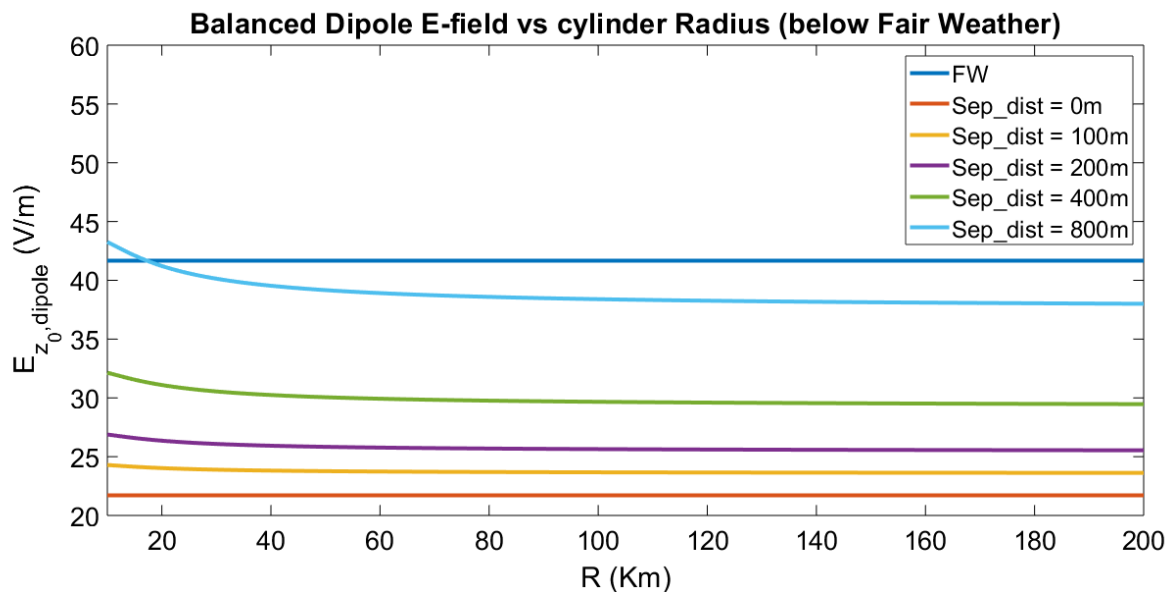
Fig. 9. Vertical electric field strength at ground level for a dipole of finite uniformly charged cylinders $E_{z_0,dipole}$, within an elevated dust layer as a function of the cylinder radius R. $E_{z_0,dipole}$ is calculated for relatively small separation distances between the charged layers. As the separation distance increases, the E-field increases due to the stronger influence of the lower cylinder to the surface resistance as it moves towards the ground, but the enhancement is not significant enough to overcome the fair weather values.
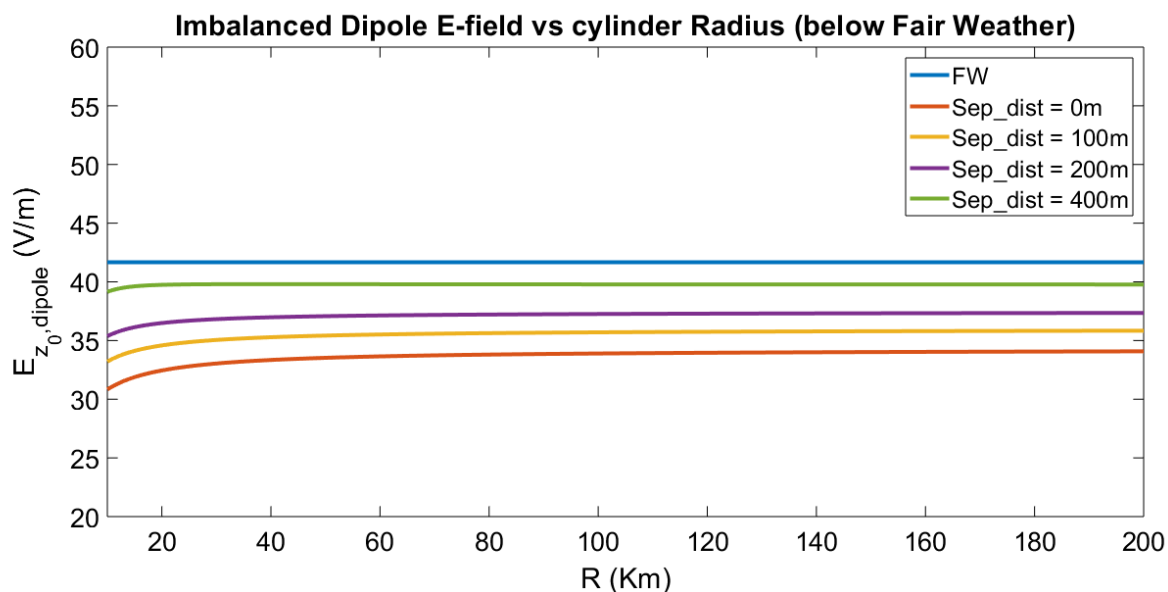
Fig. 10. Vertical electric field strength at ground level for an imbalanced dipole of finite charged cylinders $E_{z_0,dipole}$, within an elevated dust layer as a function of the cylinder radius R. $E_{z_0,dipole}$ is calculated for relatively small separation distances. Dipole exhibits charge imbalance of 8% (relative charge density difference), with the upper negative cylinder having smaller charge density. As the charged layers move apart the E-field increases more rapidly than in the case of balanced charges, for the same separation distances, since the influence of the upper cylinder is dominant. The effect is, again, not significant enough to overcome the fair weather values but the dust layer is stratified.

32

760
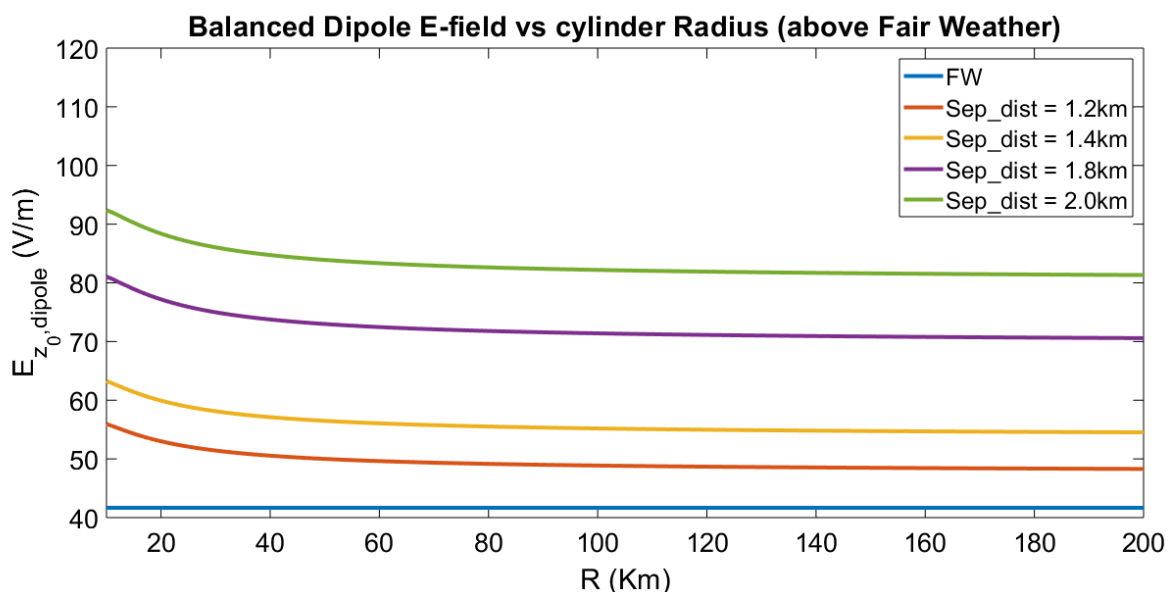
Fig. 11. Vertical electric field strength at ground level for a dipole of finite uniformly charged cylinders $E_{z_0,dipole}$, within an elevated dust layer as a function of the cylinder radius *R*. The E-field is calculated for separation distances over 1 km between the two charged layers, which results in significant enhancement of the electric field above the fair weather values. The influence of the lower cylinder 765 to the ground E-field becomes more prominent as the separation distance increases.
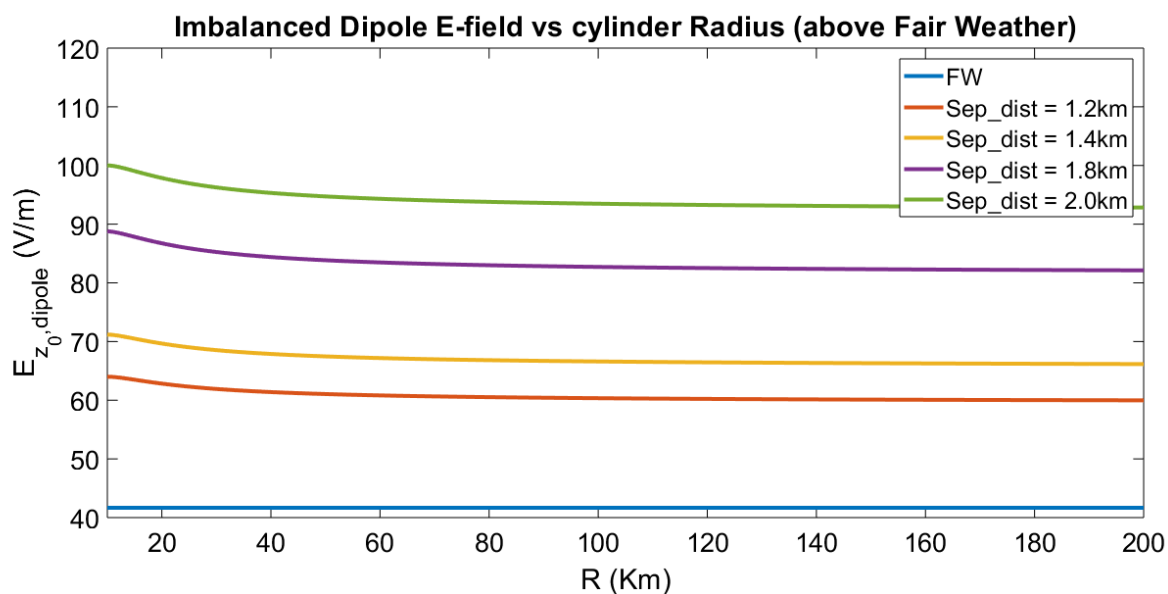

Fig. 12. Vertical electric field strength at ground level for an imbalanced dipole of finite charged cylinders $E_{z_0,dipole}$, within an elevated dust layer as a function of the cylinder radius *R*. The E-field is calculated for separation distances over 1 km between the two charged layers, which results in significant enhancement of the electric field above the fair weather values. The dipole exhibits a charge imbalance of 8%, with the upper negative cylinder having smaller charge density. For these separation distances, the effect 770 to the electric field is significant enough to overcome the calculated fair weather values.
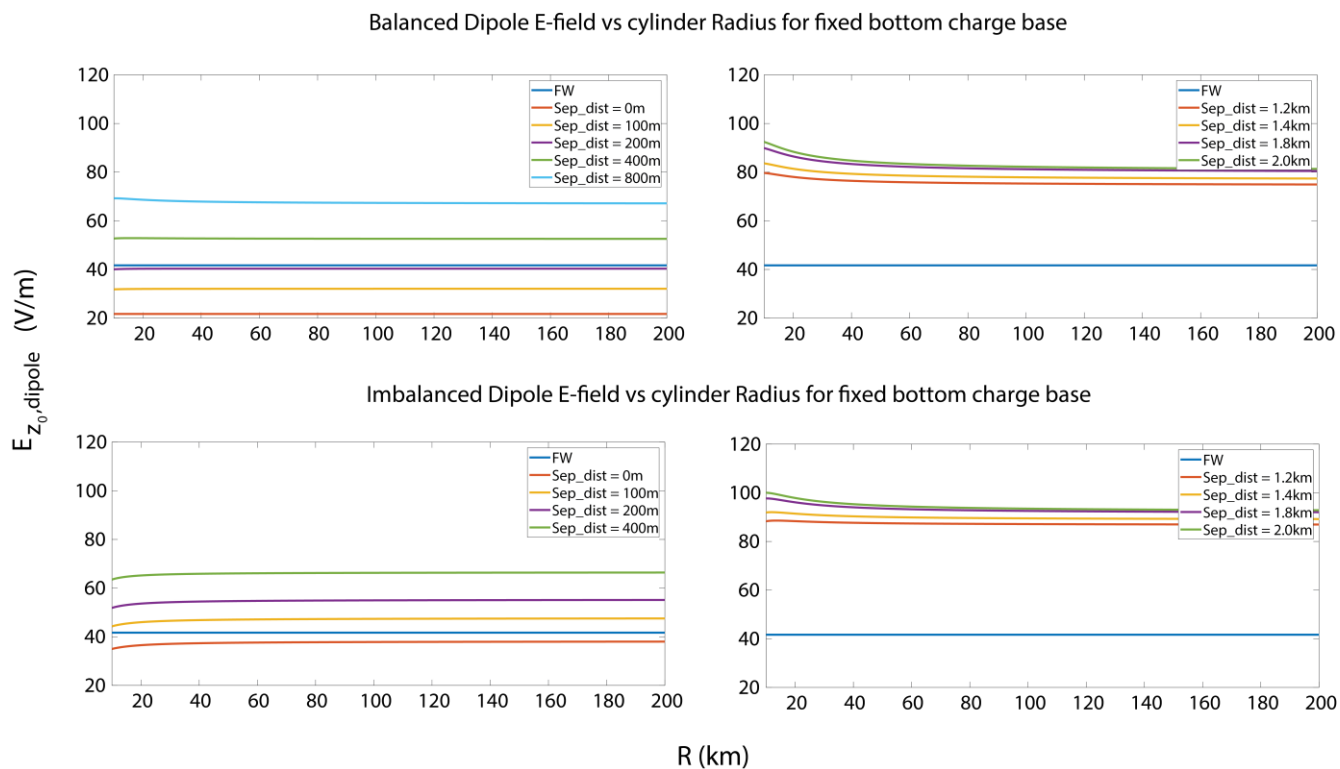
Fig. 13. Dipole electric field strength at ground level as a function of the cylinder radius R, with the bottom cylinder at 2 km fixed central height within the dust layer. The separation distance between the upper and bottom charged layer increases as the upper cylinder moves towards the top of the dust layer, for both cases of balanced and imbalanced dipoles.

775
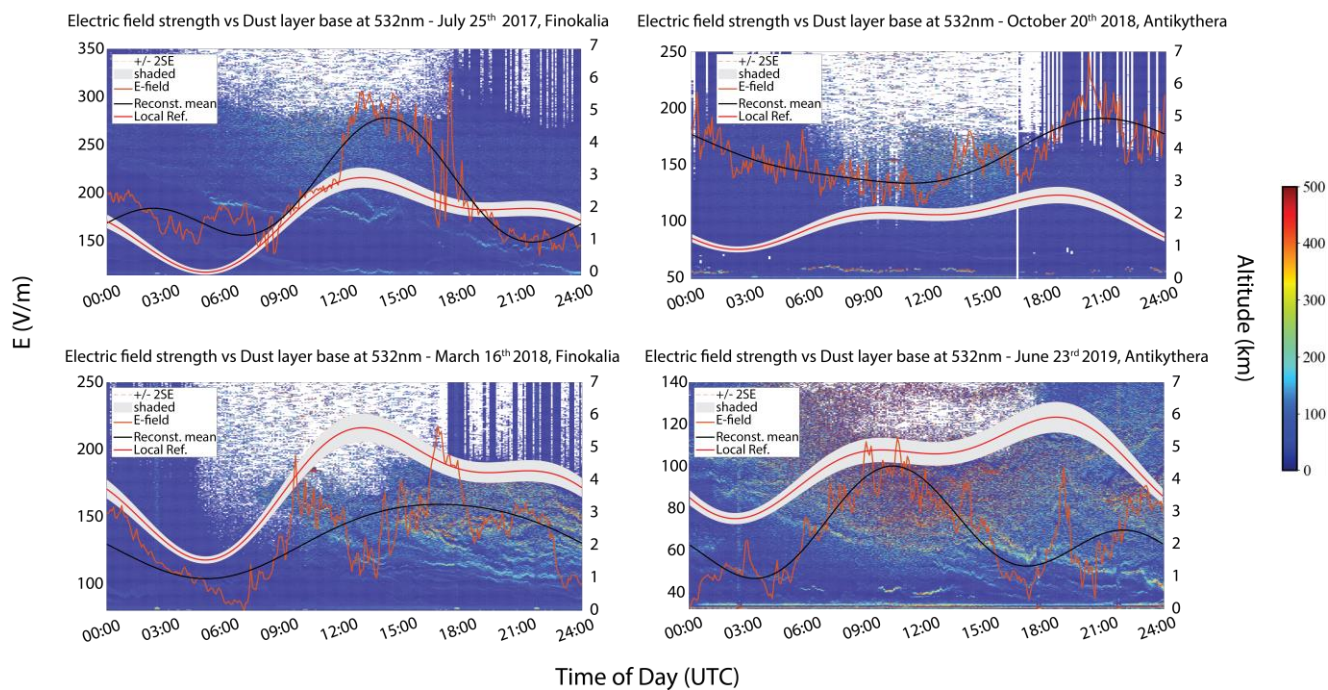
Fig. 14. Timeseries of the vertical electric field strength (orange), the Localized Reference Electric Field (red) and the reconstructed mean variation (black), plotted with the first derivative of the cross component of the attenuated backscatter coefficient at 532 nm against the altitude, for the dust cases of 25/07/2017, 20/10/2018, 16/04/2018 and 23/06/2019. The dust layer bottom base is signified by the positive maximum values of the derivative within the 0-500 colorbar range.